PAPER • OPEN ACCESS

Topological superfluidity with repulsive alkaline-earth atoms in optical lattices

To cite this article: L Isaev *et al* 2019 *New J. Phys.* **21** 073049

New Journal of Physics
The open access journal at the forefront of physics

Deutsche Physikalische Gesellschaft DPG
IOP Institute of Physics

Published in partnership with: Deutsche Physikalische Gesellschaft and the Institute of Physics

OPEN ACCESS

RECEIVED
4 February 2019

REVISED
6 May 2019

ACCEPTED FOR PUBLICATION
3 July 2019

PUBLISHED
24 July 2019

PAPER

Topological superfluidity with repulsive alkaline-earth atoms in optical lattices

L Isaev[1], A Kaufman[1], G Ortiz[2] and A M Rey[1]

[1] JILA, NIST, Department of Physics & Center for Theory of Quantum Matter, University of Colorado, 440 UCB, Boulder, CO 80309, United States of America
[2] Department of Physics and Center for Exploration of Energy and Matter, Indiana University, Bloomington IN 47405, United States of America

E-mail: ortizg@indiana.edu **and** arey@jilau1.colorado.edu

Keywords: topological superfluidity, ultra-cold atoms, Majorana modes, Sr optical lattice clock

Abstract

We discuss a realization of topological superfluidity with fermionic atoms in an optical lattice. We consider a situation where atoms in two internal states experience different lattice potentials: one species is localized and the other itinerant, and show how quantum fluctuations of the localized fermions give rise to an attraction and spin–orbit coupling in the itinerant band. At low temperature, these effects stabilize a topological superfluid of mobile atoms even if their bare interactions are repulsive. This emergent state can be engineered with alkaline-earth atoms in a superlattice with a dimerized unit cell. To probe its unique properties we describe protocols that use high spectral resolution and controllability of a narrow clock transition, such as momentum-resolved spectroscopy and supercurrent response to a synthetic (laser-induced) magnetic field.

1. Introduction

Our understanding of many-body systems traditionally relies on the Landau classification of ordered states of matter based on global symmetries spontaneously broken within a given phase. This symmetry breaking is accompanied by emergence of an order-parameter (OP), i.e. non-zero expectation value of a local physical observable that uniquely characterizes the phase. For instance a hallmark signature of a fermionic superfluid (SF) is breaking of the particle number conservation [$U(1)$] symmetry which occurs as a result of Cooper pairing. The corresponding OP plays the role of a Cooper pair wavefunction and defines an energy gap in the excitation spectrum, allowing dissipationless particle currents [1]. However, many phases of matter defy the Landau paradigm. An important class of such systems are topological superfluids (TSFs) [2, 3], i.e. phases that in addition to $U(1)$, break a residual $\mathbb{Z}_2$ symmetry. The latter symmetry breaking is a global phenomenon that occurs *in the absence of local OPs* and only for appropriate boundary conditions [4–7].

Despite all efforts dedicated to the search for TSFs, they remain elusive with the only confirmed realization being liquid ^{3}He [8, 9]. One reason for such scarcity is that TSFs require a very particular orbital structure of Cooper pairs, at least p-wave [10–12], which may originate either from strongly spin-dependent interactions, dipolar couplings [13], or a large spin–orbit coupling (SOC) that couples particle's motion to its spin.

The coexistence of a sizeable SOC and attractive interactions (leading to Cooper pairing) is quite rare in nature [14], fundamentally because SOC and fermion pairing have very different physical origins. In the present work, we propose a pathway towards topological superfluidity, which overcomes these limitations by engineering attractive interactions and an effective SOC from the same ingredient—the optical lattice structure. We study a model of repulsive fermions in two bands: one localized and another itinerant, and show that inhomogeneities spanning few lattice sites (e.g. dimerization) in the localized band lead to two profound phenomena. First, they induce an emergent *short-range* attractive interaction among the itinerant species, by virtue of local quantum fluctuations. Second, they enlarge the unit cell in accordance with the extent of localized wavefunctions. The index of non-equivalent sites within the unit cell plays the role of a spin degree of freedom

which flips whenever an atom tunnels between cells. As a result, itinerant fermions experience an effective SOC whose magnitude is comparable to the bandwidth. We show that a combination of this SOC and attractive interactions gives rise to a robust p-wave TSF in quasi-one dimension (quasi-1D) and a chiral $p_x + ip_y$ SF in 2D.

Our TSF state can be observed in ultracold *nuclear-spin polarized* fermionic alkaline-earth atoms (AEAs) [15], e.g. ^{87}Sr [16] or ^{173}Yb [17, 18], in an optical superlattice with a few-site unit cell [19–22]. The localized (itinerant) states can be implemented with atoms in an excited $^3P_0$ (ground state $^1S_0$) clock state (respectively, e- and g-states), with a *single e-atom per unit cell*. We propose several experimental probes for characterizing the TSFs, including momentum-resolved spectroscopy [23, 24] and generation of a particle supercurrent with a laser-induced synthetic magnetic field [25–27]. Our approach avoids many known experimental issues: (i) the only relevant interactions occur through the almost perfectly elastic a_{eg}^- channel [28] (when the two-atom wavefunction is antisymmetric with respect to interchange of e and g flavors, and symmetric in the spatial indices), and therefore the system is not affected by inelastic e–e losses [29, 30] or strong scattering in the e–g symmetric a_{eg}^+ channel when close to an orbital Feshbach resonance [31, 32]; (ii) p-wave interactions in our case emerge as a result of quantum fluctuations as opposed to a p-wave Feshbach resonance, and our setup is free from the three-body losses reported in experiments [33–36]; (iii) the effective SOC in our system is generated as a result of the lattice structure and hence avoids heating, inherent to earlier proposals to create SOC using near-resonant Raman lasers [37–45]. Our proposal is facilitated by the existence of magic [46] and zero-magic [47] lattices for alkaline-earth atoms at amenable wavelengths. Finally, our cold-atom system opens a path towards a long-sought-after realization of a pairing mechanism in repulsive fermions that emerges because of nanoscale inhomogeneities [48–51] and has fundamental implications for superconductivity in cuprate and heavy-fermion materials.

2. p-wave superfluidity in a quasi-1D superlattice

Key aspects of the emergent Cooper pairing and SOC leading to our proposed TSF state can be seen by studying the dimerized quasi-1D optical lattice, shown in figure 1(a) and described by the model Hamiltonian:

$$\begin{aligned}\hat{H} = &-J_e \sum_{i\,\boldsymbol{x}_\perp} (\hat{e}^\dagger_{i\boldsymbol{x}_\perp 1}\hat{e}_{i\boldsymbol{x}_\perp 2} + \text{h.c.}) + U_{eg}^- \sum_{i\,\boldsymbol{x}_\perp a} \hat{n}^e_{i\boldsymbol{x}_\perp a}\hat{n}^g_{i\boldsymbol{x}_\perp a} \\ &- J_g \sum_{i\,\boldsymbol{x}_\perp} (\hat{g}^\dagger_{i\boldsymbol{x}_\perp 1}\hat{g}_{i\boldsymbol{x}_\perp 2} + \hat{g}^\dagger_{i+1,\boldsymbol{x}_\perp 1}\hat{g}_{i\boldsymbol{x}_\perp 2} + \text{h.c.}) \\ &- J_g^\perp \sum_{i,\langle \boldsymbol{x}_\perp \boldsymbol{x}'_\perp\rangle} (\hat{g}^\dagger_{i\boldsymbol{x}_\perp a}\hat{g}_{i\boldsymbol{x}'_\perp a} + \text{h.c.}),\end{aligned} \tag{1}$$

where $i = x_i = 0, \ldots, N_d - 1$, $\boldsymbol{x}_\perp = (y, z)$ and $a = 1, 2$ labels dimers and sites within a dimer, respectively. $\langle \boldsymbol{x}_\perp \boldsymbol{x}'_\perp\rangle$ denotes nearest-neighbor links in the yz-plane. The operator $\hat{e}^\dagger_{i\boldsymbol{x}_\perp a}$ ($\hat{g}^\dagger_{i\boldsymbol{x}_\perp a}$) creates a *nuclear-spin polarized* e (g) atom at site a within a dimer with position $(i, \boldsymbol{x}_\perp)$ ($\hat{n}^e_{i\boldsymbol{x}_\perp a} = \hat{e}^\dagger_{i\boldsymbol{x}_\perp a}\hat{e}_{i\boldsymbol{x}_\perp a}$ and similarly for $\hat{n}^g_{i\boldsymbol{x}_\perp a}$). The e-atoms occupy a dimerized lattice with a large intra-dimer hopping $J_e > 0$ and one atom per dimer (we assume that dimers are decoupled). The g-atoms propagate in a simple (non-dimerized) lattice with a nearest-neighbor tunneling J_g. The second term in (1) contains a local e–g repulsion of strength $U_{eg}^- > 0$.

As we shall demonstrate below (see figure 2(d)) phases exhibited by Hamiltonian (1) are insensitive to values of $J_g^\perp$ as long as they are small compared to J_g. To simplify the presentation (and only for this reason), we consider a pure 1D case $J_g^\perp = 0$ and omit $\boldsymbol{x}_\perp$ in subscripts. However, we emphasize that our results actually apply to an anisotropic 3D system of weakly coupled 1D tubes, which is closer to what is accessible in most cold-atom experiments (see also an extension to a 2D geometry in appendix G).

We focus on the regime $J_e \gg U_{eg}^-$ and J_g when interactions and g-atom kinetic energy in (1) can be considered a perturbation to the e-atom kinetic energy. For ith dimer, the latter has eigenstates $|\lambda\rangle_i = \frac{1}{\sqrt{2}}(\hat{e}^\dagger_{i1} + \lambda\hat{e}^\dagger_{i2})|\text{vac}\rangle$ ($\lambda = \pm 1$ and $|\text{vac}\rangle$ is the vacuum state without atoms) with energies $-\lambda J_e$ (figure 1(b)). States of the entire e–g system can be approximately written as $|\Psi_{eg}\rangle = \prod_i |\lambda\rangle_i \otimes |\Psi_g\rangle$ ($|\Psi_g\rangle$ is a state of only g-atoms), thanks to the single-dimer gap $2J_e$.

We next assume that the e-subsystem is prepared in the excited state $\prod_i |\lambda = -1\rangle_i$. This configuration is stable because of the large energy penalty $2J_e$ that suppresses decay of individual dimers to their ground state (GS) with $\lambda = +1$ in the absence of decoherence sources (this requirement is well satisfied in cold-atom systems), for instance due to e–g scattering. The weak interactions U_{eg}^- only induce e-atom virtual transitions to dimer states with $\lambda = +1$, which we take into account via 2nd order perturbation theory (the kinetic energy of g-atoms amounts to a 1st order correction because it operates within the degenerate subspace $\{|\Psi_{eg}\rangle\}$). These virtual processes, shown in figure 1(c), give rise to an effective Hamiltonian for the g-subsystem (see appendix A)

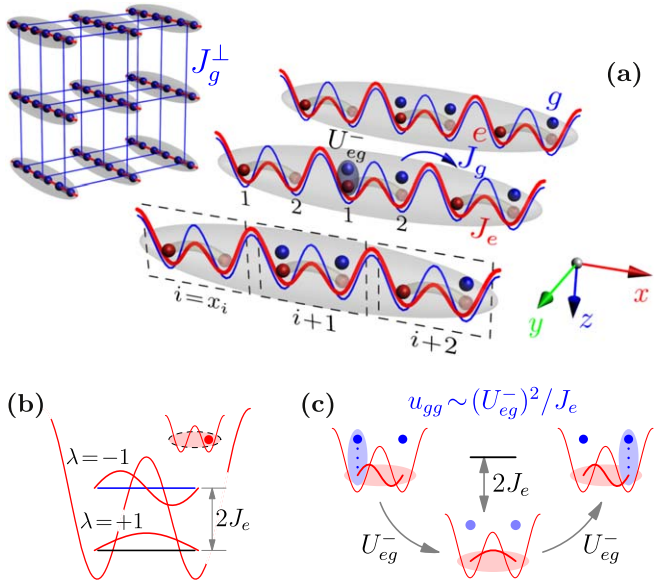

Figure 1. (a) The system described by equation (1) can be implemented by tightly confining in an array of 1D tubes (shown schematically in the inset) an ultra-cold gas of nuclear-spin polarized fermionic alkaline-earth atoms prepared in the clock states g (in blue) and e (red color). Along the tubes, e-atoms experience a superlattice that consists of weakly-coupled double-wells (dimers) with large intra-dimer tunneling J_e. The g-atoms are itinerant and experience a weaker lattice potential along the tube direction with a nearest-neighbor hopping J_g. There is also a weak inter-tube g-atom hopping $J_g^\perp$ that connects corresponding sites of dimers in nearest-neighbor tubes. We will put $J_g^\perp = 0$ until the end of section 2.1. Within each tube, a unit cell (dashed rectangle) at a position $x_i = i$ includes two lattice sites labeled with $a = 1, 2$ (4 wells overall). The e–g repulsive interaction $U_{eg}^- > 0$ is assumed small compared to J_e: $U_{eg}^- \ll J_e$. (b) Symmetric ($\lambda = +$) and antisymmetric ($\lambda = -$) e-atom kinetic-energy eigenstates within a dimer. (c) When e-atom dimers are prepared in the anti-symmetric mode, virtual transitions to the symmetric state, caused by the e–g interaction, induce an effective attraction $u_{gg} = (U_{eg}^-)^2/4J_e$ between two g-fermions within a dimer. These processes are captured by the effective model (2).

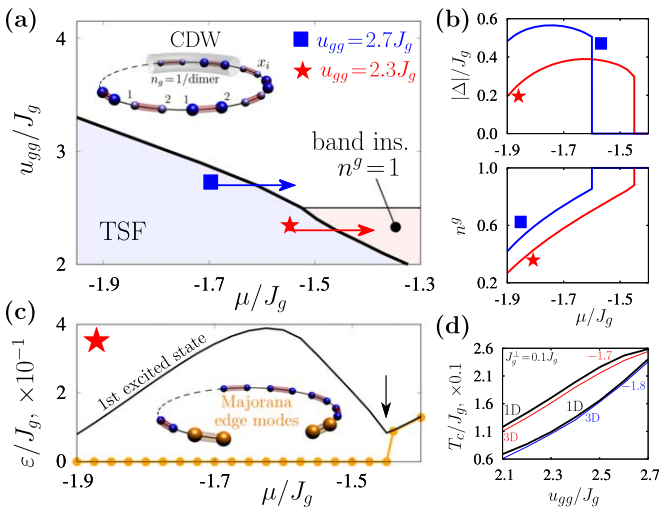

Figure 2. (a) Zero-temperature phase diagram of equation (2) computed using an unconstrained Hartree–Fock–Bogoliubov mean-field theory in a system with $N_d = 100$ dimers and periodic boundary conditions. μ is the g-atom chemical potential. Thick [thin] lines indicate 1st order transitions between topological superfluid (TSF) and insulator states [2nd order transition inside the insulating region]. In the charge-density wave (CDW) state the unit cell has two dimers with an average density $n^g = 1$ atom per dimer. For small u_{gg} the CDW undergoes a transition to a band insulator with a single-dimer unit cell. Blue square (red star) corresponds to $u_{gg}/J_g = 2.7$ (2.3). (b) SF gap Δ and average density $n^g = \frac{1}{N_d}\sum_i (n_{i1}^g + n_{i2}^g)$ plotted along the arrows shown in (a). (c) Two *lowest-magnitude* eigenvalues ε of the BdG Hamiltonian computed in an open chain for $u_{gg} = 2.3J_g$. The order parameters were taken from a converged solution in (a). Orange circles indicate Majorana edge modes inside the TSF phase. The arrow marks a TSF-band insulator transition. (d) Critical temperature T_c as a function of interaction strength u_{gg} in the strong 1D limit $J_g^\perp/J_g = 0$ (thick black lines) and anisotropic 3D case with $J_g^\perp/J_g = 0.1$ (thin red and blue lines) [see inset in figure 1(a)] for $\mu/J_g = -1.8$ (blue color) and -1.7 (red line). $N_d = 100$ [see (a)], while transverse dimensions are 60×60 tubes. The Boltzmann constant is $k_B = 1$.

$$\hat{H}_{\rm ef} = \hat{H}_0^g - u_{gg}\sum_i \hat{n}_{i1}^g \hat{n}_{i2}^g,$$
$$\hat{H}_0^g = -J_g \sum_k [\sigma^x(1+\cos k) + \sigma^y \sin k]_{ab}\, \hat{g}_{ka}^\dagger \hat{g}_{kb}, \quad (2)$$

where $\hat{g}_{ka} = \frac{1}{\sqrt{N_d}}\sum_i e^{-ikx_i}\hat{g}_{ia}$, $\boldsymbol{\sigma}$ are Pauli matrices, momentum $k \in [-\pi, \pi]$ (in units of inverse lattice spacing $1/a_0$) is defined in a dimer Brillouin zone (BZ) with N_d states. $u_{gg} = (U_{eg}^-)^2/4J_e$ is the strength of intra-dimer g-atom attraction mediated by quantum fluctuations of localized e-atoms[3]. If we associate the site index $a = 1, 2$ inside a dimer with a spin-$\frac{1}{2}$ degree of freedom, $\hat{H}_0^g$ contains kinetic energy with a SOC that arises because any tunneling event 'flips' pseudospin a. This effective Hamiltonian will give rise to a TSF phase.

The physical origin of the p-wave TSF phase is especially transparent at weak coupling $u_{gg} \ll J_g$ and low filling $n^g \ll 1$, when the kinetic energy in (2) dominates and is diagonalized by states $\hat{f}_{k\tau} = \frac{1}{\sqrt{2}}(\hat{g}_{k1} - \tau e^{-i\frac{k}{2}}\hat{g}_{k2})$ with energies $\epsilon_k = 2\tau J_g \cos\frac{k}{2}$ ($\tau = \pm 1$). In a dilute system, the Fermi sea occupies states with small momenta $|k| \ll \pi$ in the low-energy $\tau = -1$ band, and to an excellent approximation we can keep only the $\hat{f}_{k,-1} \equiv \hat{f}_k$ mode. As a result, interactions in (2) become manifestly p-wave (see [52]):

$$\hat{H}_{\rm ef} \approx \sum_k \epsilon_k \hat{f}_k^\dagger \hat{f}_k - \frac{u_{gg}}{4N_d}\sum_{k'kq} e^{i\frac{q}{2}}\hat{f}_{k+q}^\dagger \hat{f}_{k'-q}^\dagger \hat{f}_{k'}\hat{f}_k. \quad (3)$$

Within the Bogoliubov mean-field theory (see appendix B) one introduces a pairing OP

$$\Delta = -\frac{u_{gg}}{4N_d}\sum_q e^{-i\frac{q}{2}}\langle \hat{f}_{-q}\hat{f}_q\rangle,$$

which parameterizes the single-particle excitation spectrum

$$E_k = \sqrt{(\epsilon_k - \mu)^2 + |D_k|^2},$$

with a p-wave gap $D_k \approx i\,k\Delta$. μ is the g-atom chemical potential (set by the Fermi energy). Δ is a solution of the self-consistency equation $1 = \frac{u_{gg}}{16N_d}\sum_k \frac{k^2}{E_k}$, $\Delta \approx J_g e^{-2\pi J_g/u_{gg}\sqrt{1-(\mu/2J_g)^2}}$.

Physical origins of the Hamiltonian (3) and the p-wave superfluid state are similar to the mechanism of singlet-triplet mixing in s-wave superconductors with Rashba SOC [25, 53–56] due to broken spin $SU(2)$ symmetry.

2.1. Stability and topological nature of the superfluid state

To assess the stability of the p-wave SF state beyond the weak coupling limit, and uncover its topological properties, we compute the phase diagram of $\hat{H}_{\rm ef}$ within a fully unconstrained Hartree–Fock–Bogoliubov (HFB) mean-field approach in real space (explained in appendix C). This variational technique minimizes the grand potential $\langle \hat{H}_{\rm ef} - \mu\sum_{ia}\hat{g}_{ia}^\dagger \hat{g}_{ia}\rangle$ (μ is the g-atom chemical potential) with respect to local OPs $\Delta_i = -u_{gg}\langle \hat{g}_{i2}\hat{g}_{i1}\rangle$, $\xi_i = \langle \hat{g}_{i2}^\dagger \hat{g}_{i1}\rangle$ and $n_{ia}^g = \langle \hat{g}_{ia}^\dagger \hat{g}_{ia}\rangle$, and includes the competition between SF phases with a finite gap Δ_i and various inhomogeneous states, e.g. charge-density waves (CDWs) and magnetic phases, characterized by a site-dependent n_{ia}^g and ξ_i, respectively. The minimization is performed at zero temperature $T = 0$ in a system with periodic boundary conditions (BCs). Once the GS is self-consistently determined, we open the chain and diagonalize the Bogoliubov-de Gennes (BdG) mean-field Hamiltonian *with fixed OPs* to determine edge modes: If an SF phase displays zero-energy (Majorana) modes, we call it topological [2]. Figure 2(a) shows the phase diagram of model (2) as a function of chemical potential μ and interaction u_{gg}. In agreement with the previous section, the SF phase is stable at weak coupling $u_{gg} < J_g$ and low density, and is characterized by the mixing of singlet $\langle \hat{g}_{-k,2}\hat{g}_{k1}\rangle$ and triplet $\langle \hat{g}_{-k,a}\hat{g}_{ka}\rangle$ Cooper pair amplitudes. To better understand this effect, let us consider properties of the model (2) under space inversion I: $x \to -x$. In the dimerized lattice, $I = \sigma^x \otimes I_d$, where I_d: $k \to -k$ is an inversion acting on the dimer center-of-mass and σ^x appears because I must interchange dimer sites. The SOC $\hat{H}_0^g$ is invariant under I but *manifestly breaks* I_d due to the odd-momentum terms. In an SF state, Cooper pair wavefunctions inherit this feature and the system exhibits p-wave pairing between same-flavor g-atoms $\langle \hat{g}_{-k,a}\hat{g}_{ka}\rangle \sim k^n$ (n is odd) despite the s-wave nature of interactions in equation (2). We again note a similarity of this situation and singlet-triplet mixing in non-centrosymmetric superconductors with Rashba SOC [14, 25, 26].

When u_{gg} or μ is increased, the system undergoes a 1st order transition to a non-SF gapped state with an average density $n^g = 1$ (figure 2(b)). This phase is a band insulator for small u_{gg}, and a CDW with two dimers per unit cell for strong interactions. As shown in figure 2(c), the SF state is *topological* (i.e. possesses zero-energy edge modes) for all u_{gg} and μ where it is stable. This happens because we used the Hartree–Fock OPs in our variational scheme: if the minimization were constrained to include only site-independent Δ_i, one would

[3] Note that u_{gg} is small compared to J_e, but the ratio u_{gg}/J_g can be arbitrary.

recover a well-known transition [2] from TSF to a non-topological SF state. The latter phase is unstable towards CDW formation and the transition never happens.

The phase diagram in figure 2(a) remains valid at finite temperature $T > 0$. Indeed, as demonstrated in figure 2(d) a typical critical temperature, above which the SF phase disappears, is $T_c \sim 0.1J_g$ (here and below we use the units with Boltzmann constant $k_B = 1$). For $T > T_c$, the system becomes a homogeneous Fermi liquid.

It is important to emphasize that we focused on the 1D case only for simplicity, and our results really apply to a 3D system with anisotropic g-atom hopping, shown in the inset of figure 1(a). To demonstrate this, we add a weak transverse nearest-neighbor hopping $J_g^\perp$ of g-atoms in the yz-plane between corresponding sites of the dimers and compare the critical temperature obtained using the 3D HFB approximation with the 1D case. The transverse hopping processes are described by an additional term in the Hamiltonian (2):

$$\delta\hat{H}_0^g = \sum_{\boldsymbol{k}} \epsilon_{\boldsymbol{k}}^\perp \delta_{ab}\, \hat{g}_{\boldsymbol{k}a}^\dagger \hat{g}_{\boldsymbol{k}b}$$

with $\epsilon_{\boldsymbol{k}}^\perp = -2J_g^\perp(\cos k_y + \cos k_z)$, $\boldsymbol{k} = (k, k_y, k_z)$ and $\hat{g}_{\boldsymbol{k}a} \equiv \hat{g}_{kk_y k_z a}$. Replacing $\hat{H}_0^g \to \hat{H}_0^g + \delta\hat{H}_0^g$, we obtain the function $T_c(u_{gg})$ for 1D ($J_g^\perp = 0$) and 3D ($J_g^\perp = 0.1J_g$) lattices, presented in figure 2(d). Adding a relatively weak $J_g^\perp$ only slightly perturbs the results of the strictly 1D calculation. Moreover, it is known [57] that Majorana modes also remain unchanged in a system of weakly-coupled 1D tubes. Therefore, in the rest of the paper we continue studying the 1D system with $J_g^\perp = 0$.

2.2. Topological superfluid phase beyond mean-field: fermion parity switches

Although our analysis so far utilized the HFB approximation, the topological nature of the SF state remains intact even when corrections beyond that mean-field approach are taken into account. By the Mermin–Wagner theorem, compact, continuous symmetries cannot be spontaneously broken in one dimension, for systems with finite-range interactions. That means that the $U(1)$ symmetry of particle-number conservation cannot be broken spontaneously in our strictly one-dimensional system. Nonetheless, in a finite system one can still draw conclusions about the topological nature of the system's ground state. To this end, we are going to investigate the behavior of the many-body fermion parity switch [4, 5], a topological invariant that signals the presence of a topologically non-trivial superfluid phase in our system. This invariant reveals the physical emergence of a fractional (4π-periodic) Josephson effect response.

To demonstrate the topologically non-trivial nature of the phase, we compute the fermion parity switch

$$\mathcal{X} = \tfrac{1}{2N}[E_0(N_g + 1) + E_0(N_g - 1)] - \tfrac{1}{N}E_0(N_g) \tag{4}$$

with $N = 2N_d$, $E_0(N_g)$—the GS energy of the Hamiltonian (2) with N_g fermions (we assume N_g even) using exact diagonalization in a single tube (1D dimerized lattice), and show that it changes sign when the boundary conditions are switched from periodic to anti-periodic. When this happens, the GS realizes a fermionic parity switch [4, 5] for a given N_g.

In figure 3 we present exact diagonalization results (using the Lanczos technique of [58]) in systems with $N = 26$ sites (13 dimers), and an even number of g-atoms $N_g = 2, \ldots, 10$. Clearly, $\mathcal{X}$ displays different signs for the two types of boundary conditions, thus realizing the fermion parity switch, indicating the topologically non-trivial nature of the phase.

3. Preparation in ultra-cold gases

The system in figure 1(a) and equation (1) can be realized with AEAs, such as fermionic ^{87}Sr, using the sequence of steps shown in figure 4: Step (0) We start with a nuclear-spin polarized g-atom band insulator (in the lowest lattice band) in a deep magic-wave lattice (where e and g atoms experience equal light shifts and therefore same trapping potential [46]) with suppressed tunneling. Step (1) The system is irradiated by a laser with a staggered phase (equal to π) and resonant with the $|g0\rangle \to |e1\rangle$ transition [$|g(e)n\rangle$ denotes a $g(e)$-atom in the lattice band n]. The laser intensity is adjusted to perform a $\frac{\pi}{2}$-pulse that turns states $|g0\rangle$ into $|g0\rangle \pm |e1\rangle$ at neighboring lattice sites. Step (2) is another $\frac{\pi}{2}$-pulse similar to the previous step, but with a uniform phase of 2π. As a result, states $|g0\rangle + |e1\rangle$ evolve back to $|g0\rangle$, while $|g0\rangle - |e1\rangle$ become $|e1\rangle$.

Steps (3) and (4) are the most difficult because an adiabatic protocol needs to be implemented. First, we create a dimerized e-superlattice by ramping up a potential experienced only by e-atoms [47] at twice the periodicity of the magic lattice, and apply a π-pulse to resonantly transfer the states $|e1\rangle$ to excited antisymmetric motional states in each double-well, in order to satisfy $|J_e| > |J_g|$ [59]. Second, we prepare a g-atom Fermi-liquid state starting from the CDW state in step (2). This is accomplished by applying a large energy bias $\Delta_0 = \Delta$ ($t = 0$) to wells that contain g-atoms, which makes this CDW the g-subsystem GS. This state can be adiabatically transferred to the GS of delocalized g-atoms by decreasing Δ until it vanishes and at the same time varying the

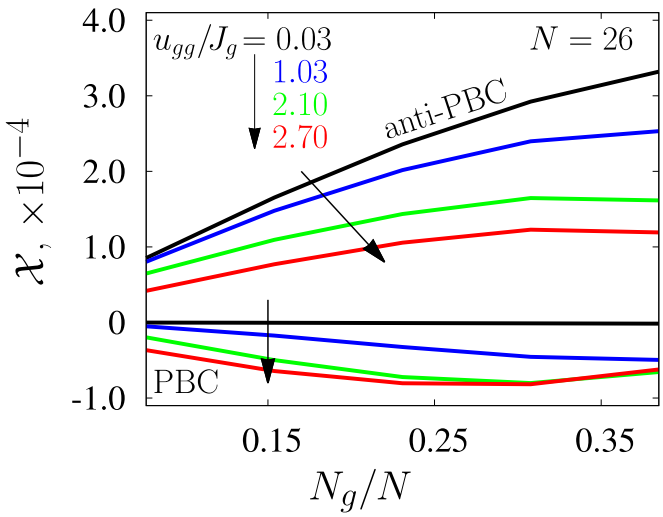

Figure 3. Fermion parity switch $\mathcal{X}$ (4) of a chain with periodic and anti-periodic boundary conditions (PBC and anti-PBC) computed using Lanczos exact diagonalization in a chain with $N = 26$ sites. The number of g-atoms is even: $N_g = 2, \ldots, 10$. Blue, cyan, green and red curves correspond to interaction strengths $u_{gg}/J_g = 0.03, 1.03, 2.1$ and 2.7, respectively. Arrows show direction of increasing u_{gg}.

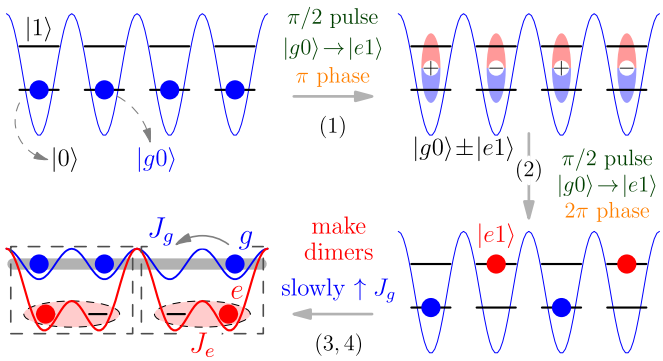

Figure 4. A protocol to prepare the model in figure 1(a) and equation (1). Blue (red) color indicates g (e) atoms. Atoms are nuclear-spin polarized and hoppings are quenched until steps (3) and (4). $|e\,(g)\;n\rangle$ means a state with one e (g) atom in the nth spatial level ($n = 0$ means GS). At step (2), pale blue-red ($\pm$) ellipses correspond to $|g0\rangle \pm |e1\rangle$ states.

hopping J_g (figure 5(a)). To illustrate this procedure (ramp), we assume that

$$\Delta(t) = \begin{cases} \Delta_0 \tanh[\gamma(t - t_0)], & t < t_0 \\ 0, & t \geqslant t_0 \end{cases}$$

and

$$J_g = J_g^{(0)} + J_m \mathrm{e}^{-\alpha(t-t_0)^2}$$

with $J_m \gg J_g^{(0)}$, and compute the wavefunction $|\psi_g(t)\rangle$ of g-atoms. The ramp stops at $t = t_f$. The overlaps $P(t) = |\langle\psi_g(t)|\mathrm{FS}\rangle|$ with the ideal Fermi sea $|\mathrm{FS}\rangle$ are presented in figure 5(b) for representative values of the parameters $J_g^{(0)}, J_m, \Delta_0, \alpha$ and γ, and several chain lengths L. As one would expect, the system exhibits an 'orthogonality catastrophe' [60] when $P(t_0)$ decays exponentially with system size due to the presence of a small number of defects in the resulting momentum distribution $n_k(t_f)$. Nevertheless, the latter is very close to the ideal Fermi function n_k^{ideal}, differing from it only near band edges (figure 5(c)).

After this last step, the filling of g-atoms can be controlled spectroscopically and the system is cooled down by removing atoms from k-states near band edges with a laser which drives a narrow transition whose detuning is adiabatically changed to scan the conduction band and access atoms deeper in the Fermi sea [59]. We anticipate, that if the atom removal can be done slow enough compared to the thermalization time set by the effective interactions between g-atoms mediated by the background e-atoms and without introducing extra heating, it should be possible to cool down the gas into the SF state.

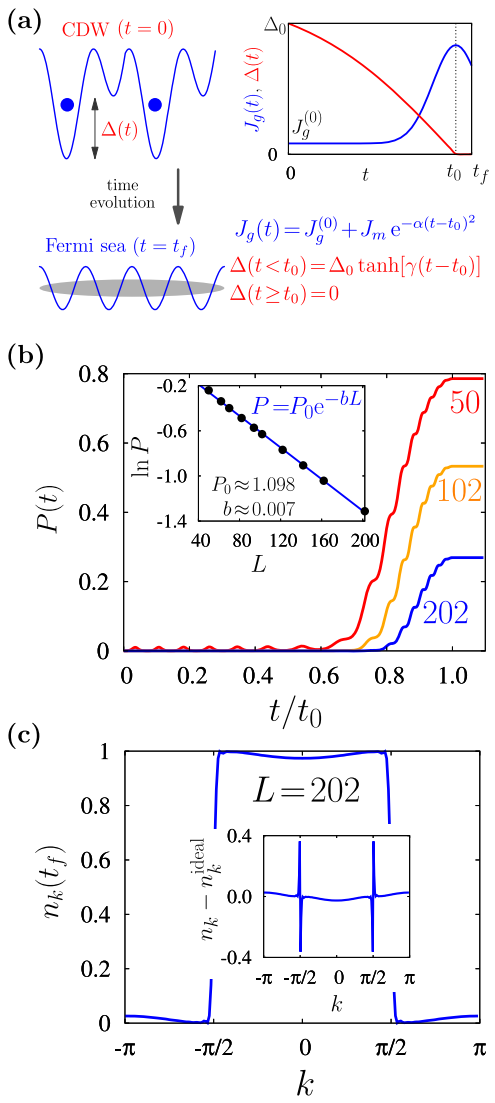

Figure 5. Adiabatic preparation (ramp) of the g-atom Fermi-liquid GS from a band insulator during steps (3) and (4) in figure 4. (a) Schematics of the ramp. $\Delta(t)$ and $J_g(t)$ are bias of g-atom wells and their hopping, respectively. (b) Overlap $P = |\langle\psi_g(t)|\mathrm{FS}\rangle|$ of the g-atom state $|\psi_g(t)\rangle$ with the ideal Fermi sea $|\mathrm{FS}\rangle$ as a function of time t and for several chain length L (indicated by numbers near curves). Parameters of the system are $t_0 J_g^{(0)} = 7.31$, $\Delta_0/J_g^{(0)} = -15$, $\alpha/[J_g^{(0)}]^2 = 0.49$, $\gamma/J_g^{(0)} = 0.15$. The inset in this panel shows finite-size scaling of $P(t_f)$ with L. (c) Momentum distribution n_k in the state $|\psi_g(t_f)\rangle$ and its deviation from $n_k^{\rm ideal}$ in $|\mathrm{FS}\rangle$.

The above scheme can be extended to realize the anisotropic 3D lattice shown in figure 1(a) and studied in section 2.1. Indeed, because all atoms are nuclear-spin polarized, we only need to add magic optical lattices along y- and z-axes. Then g-atoms will tunnel between nearest-neighbor tubes, while the hopping of e-atoms is prohibited by the Pauli exclusion principle: the only resonant states in the neighboring tubes are antisymmetric double-well orbitals which can not be doubly occupied in the absence of spin-flip tunneling processes.

4. Detection

The simplest way to verify the presence of g-atom attractive interactions u_{gg} in a cold-atom experiment, is to study quench dynamics in the *normal*, i.e. non-SF state, using the following protocol: (i) for times $t < 0$, g-atoms fill a non-interacting Fermi sea, which can be achieved by preparing a dilute system in a shallow lattice with negligible g-atom interactions u_{gg}. (ii) At $t = 0$, J_g is switched off (e.g. by increasing the lattice depth), and g-atoms are brought in contact with e-atoms, thus allowing them to experience the e–g interactions described in equation (1). Then, one lets the system evolve for a time t_0. As a result, basis states with doubly occupied dimers accumulate a phase $-Ut_0$, where U [$=-u_{gg}$ in equation (2)] is the induced g-atom interaction. (iii) At $t = t_0$, the e-atoms are removed, hopping J_g is restored and the system evolves with a non-interacting Hamiltonian (1st term in (2)). The sign of U can be determined by measuring an average number of doubly occupied dimers:

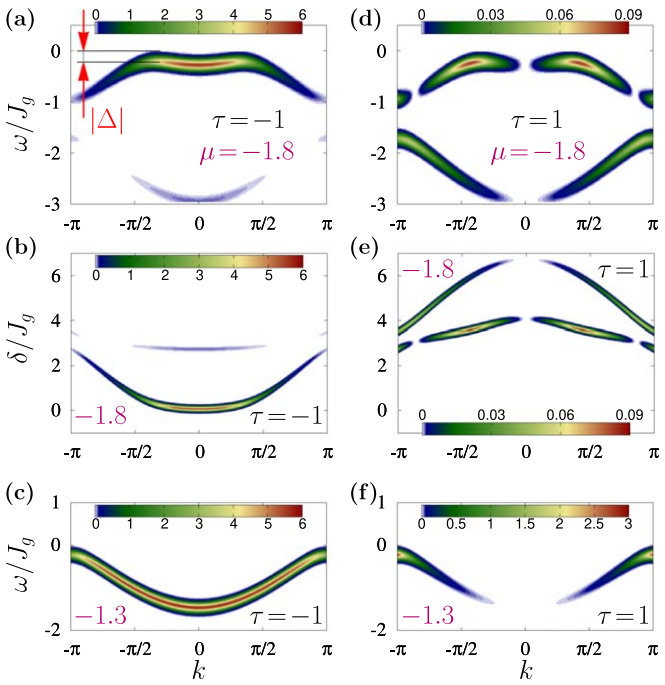

Figure 6. The transfer rate $\mathcal{R}_\tau(\delta,\, k)$ (in arbitrary units) of g-atoms from the TSF with $\mu = -1.8J_g$, and from the insulator with $\mu = -1.3J_g$ (see figure 2(a)). These values of μ are indicated by numbers in magenta. The interaction strength is $u_{gg} = 2.3J_g$. For concreteness, in the empty tube we assume $J_e = J_g$ and $\eta = 1$, so that the e-atom band structure is $\epsilon^e_{k\tau} = 2\tau J_g \cos\frac{k}{2}$. The left (right) column corresponds to $\tau = \mp 1$. (a) and (d) $\mathcal{R}_\tau$ as a function of the shifted frequency $\omega = \epsilon^e_{k\tau} - \mu - \delta$, which reveals the BdG band structure and allows us to extract the SF gap Δ. (b) and (e) The signal in the detuning-momentum plane, as it would be measured in a real experiment. (c) and (f) Same as in panels (a) and (d), but inside the band insulator with a fully filled *single-particle* band $\epsilon_{k,-1}$. A weaker signal for $\tau = 1$ is due to Hartree–Fock corrections.

$$n_2(t) = \langle\psi(t)|\sum_i \hat{n}^g_{i1}\hat{n}^g_{i2}|\psi(t)\rangle$$

in the state $|\psi(t)\rangle$ of the system at time t. For short evolution times, when $|U|t_0 \ll 1$ and $t - t_0 \ll 1/J_g$, $n_2(t) = n_2(0) - \zeta U\cdot(t - t_0)$ with $\zeta > 0$. Hence, the number of double occupancies decreases (increases) for the repulsive (attractive) interaction U [see appendix D for a complete derivation of this result].

The spectrum of Bogoliubov excitations can be probed by momentum-resolved spectroscopy [23, 24, 59]. Let us assume that we isolate a single layer of tubes along the $y = 0$ plane and remove all other tubes. A laser with a wavevector along the x-axis, Rabi frequency Ω, detuned by δ from the atomic e–g transition, transfers g-atoms from the SF phase to e-states in empty nearest-neighbor tubes along the positive y-direction (the transfer happens along the y-axis and does not change an atom's x-position along the tube, nor its z-component). The e-lattice depth has been reduced to make flat bands at $\pm J_e$ (see figure 1(b)) dispersive with a band structure $\epsilon^e_{k\tau} = \tau J_e\sqrt{1 + \eta^2 + 2\eta\cos k}$ where $\tau = \pm 1$ and ηJ_e is the inter-dimer hopping. The g-atom transfer rate to an e-band $\epsilon^e_{k\tau}$, $\mathcal{R}_\tau(\delta,\, k)$, can be written in terms of the spectral density $\mathcal{A}_{ab}(\omega,\, k)$ of the single-particle normal Green function [24]:

$$\mathcal{R}_\tau(\delta,\, k) = \frac{\Omega^2}{2}\left[\mathcal{A}_{11}(\omega,\, k) + \mathcal{A}_{22}(\omega,\, k) - 2\tau\frac{\mathrm{Re}\,[(1 + \eta e^{ik})\mathcal{A}_{12}(\omega,\, k)]}{\sqrt{1 + \eta^2 + 2\eta\cos k}}\right],$$

with $\omega = \epsilon^e_{k\tau} - \mu - \delta$ and

$$\mathcal{A}_{ab}(\omega,\, k) = i\, f(\omega)[\langle\hat{g}_{ka}\hat{g}^\dagger_{kb}\rangle_{\omega+i0} - \langle\hat{g}_{ka}\hat{g}^\dagger_{kb}\rangle_{\omega-i0}].$$

$f(\omega) = (e^{\omega/T} + 1)^{-1}$ is the Fermi function at temperature T, and i0 is an infinitesimal imaginary number (see appendix E).

The representative signal $\mathcal{R}$ is shown in figure 6. Its maximum (for a fixed k) occurs when ω coincides with the highest occupied BdG energy state. Therefore, one can map out the BdG band structure and extract the excitation gap Δ (see panels (a) and (d)). In figures 6(b) and (e) we plot the same signal as a function of the bare laser detuning δ, as it would be observed in an experiment. This spectroscopy technique can also be used to probe the insulating phase in figure 1(a). The transfer rate inside the band insulator regime is shown in figures 6(c) and (f). In this case, the excitation spectrum is again gapped, but as opposed to the SF state, this gap exists because all *single-particle* states below the Fermi level are filled, and not due to fermion pairing. Finally, we

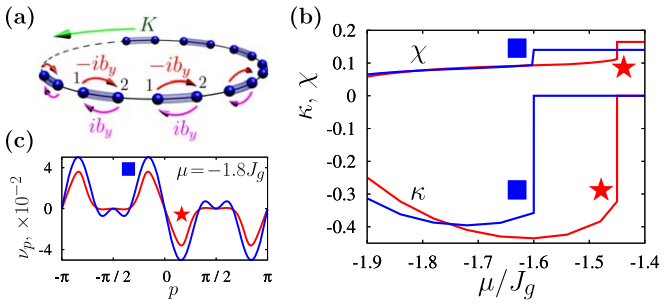

Figure 7. (a) Model (2) with a laser-assisted intra-dimer tunneling $\pm \mathrm{i}\, b_y$ simulating a magnetic field $\boldsymbol{B} = b_y \boldsymbol{e}_y$. A supercurrent $\langle \hat{K} \rangle \sim b_y$ is induced in the TSF phase. (b) Magneto-electric response $\kappa = \langle \hat{K} \rangle / b_y$ and longitudinal susceptibility $\chi = \langle \hat{S}^y \rangle / b_y$ as functions of the chemical potential μ. (c) Momentum distribution asymmetry ν_p inside the TSF phase for $b_y = 0.3 J_g$ and $\mu = -1.8 J_g$. In (b) and (c), a red star (blue square) corresponds to $u_{gg}/J_g = 2.3$ (2.7) (see figure 2).

note that the signal with $\tau = -1$ (panels (a)—(c)) is significantly stronger than the one with $\tau = 1$ ((d)—(f)), which highlights the validity of the effective model (3).

Due to the SOC inherent in equation (2), the TSF state has remarkable features that set it apart from a usual s-wave SF and can be used as its 'fingerprint'. Perhaps its most revealing property is an analog of the spin-galvanic effect, when an applied Zeeman magnetic field induces a bulk supercurrent [26, 27]. Since the pseudospin degrees of freedom in $\hat{H}_{\mathrm{ef}}$ correspond to a site index inside the unit cell, this 'field' must couple to the motion of g-atoms and can be implemented as a laser-assisted tunneling within dimers [37, 38]. This hopping can be set to have an arbitrary phase θ, but we focus on the case $\theta = \frac{\pi}{2}$, i.e. consider the perturbation:

$$\delta \hat{H}_{\mathrm{ef}} = -b_y \sum_{i,ab} \sigma^y_{ab}\, \hat{g}^\dagger_{ia} \hat{g}_{ib},$$

and compute the supercurrent response (figure 7(a))

$$\langle \hat{K} \rangle = \kappa\, b_y.$$

We can anticipate this response based on pure symmetry arguments: as explained in section 2.1, the SOC breaks the space inversion symmetry in the dimer lattice due to odd in momentum terms $\sim \sin k$. On the other hand, the synthetic Zeeman term $\delta \hat{H}_{\mathrm{ef}}$ with $b_y \neq 0$ violates time-reversal symmetry (see discussion in appendix F). Breaking of these two symmetries is a necessary condition to stabilize a state with a non-zero current in the system.

The operator $\hat{K}$ is a single-particle mass current, obtained by varying the Hamiltonian $\hat{H}_b = \hat{H}^g_0 + \delta \hat{H}_{\mathrm{ef}}$ (see equation (2)) w.r.t. the flux φ piercing the ring: $\hat{K} = \delta \hat{H}_b / \delta \varphi|_{\varphi=0}$. This flux enters via a phase factor $\mathrm{e}^{\mathrm{i}\varphi}$ on each physical link in the lattice with one-site unit cell, but in the dimerized lattice one must replace $\hat{g}_{i1} \to \mathrm{e}^{\mathrm{i}2x_i\varphi} \hat{g}_{i1}$ and $\hat{g}_{i2} \to \mathrm{e}^{\mathrm{i}(2x_i+1)\varphi} \hat{g}_{i2}$, because the position x in a non-dimerized lattice is $x = 2x_i + a - 1 = 0, \ldots, 2N_d - 1$ and $\hat{g}_x = \hat{g}_{ia}$. We obtain

$$\hat{K} = \frac{1}{N_d} \sum_k [\sigma^y (1 - \cos k) + \sigma^x (\sin k - b_y/J_g)]_{ab}\, \hat{g}^\dagger_{ka} g_{kb}.$$

In figure 7(b) we show the magneto-electric coefficient κ as a function of the chemical potential for several interaction strengths. Remarkably, κ exists *only inside* the SF phase and vanishes across the TSF-insulator transition.

Due to the p-wave nature of the SF phase, the synthetic field b_y induces a pseudospin polarization

$$\langle \hat{S}_y \rangle = \chi b_y,$$

where $\hat{S} = \frac{1}{2N_d} \sum_i \boldsymbol{\sigma}_{ab} \hat{g}^\dagger_{ia} \hat{g}_{ib}$. The susceptibility χ and magneto-electric coefficient κ can be related in the weak-coupling dilute limit $u_{gg} \ll J_g, n^g \ll 1$ at $T = 0$ [25]. Indeed, as explained in appendix F, similar calculations that led to equation (3) yield $\kappa = -4\chi = -\frac{1}{2J_g N_d} \sum_k \left[1 - \frac{\epsilon_k - \mu}{E_k}\right] \cos \frac{k}{2}$ with ϵ_k and E_k defined after equation (3). Figure 7(b) shows χ and κ as functions of the chemical potential μ across the TSF-insulator transition. In cold-atom experiments it is possible to measure χ, for example by a Ramsey-type protocol [61]: Assuming that the system is in its GS $|\psi_0\rangle$ (with $b_y \neq 0$), at $t = 0$ we quench the Hamiltonian from (2) to $\hat{H}_x = J_g \hat{S}_x$ e.g. by making the intra-dimer g-atom tunneling dominant and let the system evolve for a time $t_0 = \frac{\pi}{2J_g}$. As a result, the state becomes $|\psi\rangle = \mathrm{e}^{-\mathrm{i}\frac{\pi}{2}\hat{S}_x} |\psi_0\rangle$. Now we measure the difference in populations on two sites of a dimer, i.e. $\langle \psi | \hat{S}_z | \psi \rangle$. Because $\mathrm{e}^{\mathrm{i}\frac{\pi}{2}\hat{S}_x} \hat{S}_z \mathrm{e}^{-\mathrm{i}\frac{\pi}{2}\hat{S}_x} = \hat{S}_y$, the above protocol yields $\langle \psi_0 | \hat{S}_y | \psi_0 \rangle$ and can be used to obtain χ.

Another physical effect induced by $\delta\hat{H}_{\rm ef}$ is an asymmetry of the g-atom momentum distribution which can be detected in time-of-flight experiments [62]. Because these measurements involve the crystal momentum p in the BZ of a *single-site* unit cell, we need to compute $\nu_p = \frac{J_s}{b_y}\langle \hat{g}_p^\dagger \hat{g}_p - \hat{g}_{-p}^\dagger \hat{g}_{-p}\rangle$ with $\hat{g}_p \equiv \frac{1}{\sqrt{2N_d}}\sum_x e^{-ipx}\hat{g}_x = \frac{1}{\sqrt{2N_d}}\sum_{ia} e^{-2ipx_i - ip(a-1)}\hat{g}_{ia} = \frac{1}{\sqrt{2}}(g_{2p,1} + e^{-ip}g_{2p,2})$. Figure 7(c) shows ν_p computed in the TSF phase of figure 2(a). For comparison, in a non-SF system, $\nu_p \sim \delta_{k,k_F} - \delta_{k,-k_F}$ (k_F is the Fermi momentum). SF correlations destroy Fermi points and lead to a finite asymmetry even away from $k = \pm k_F$.

5. Discussion

Topological superfluidity in Fermi liquids is intimately related to the coupling between particles' spin and orbital motion. From this perspective, a key ingredient in our theory is the presence of lattice modulations that host localized degrees of freedom and play a dual role. On the one hand, quantum fluctuations of localized fermions stabilize superfluid states in the itinerant channel, *even when the bare interactions are repulsive*. On the other hand, the modulations enlarge the lattice unit cell and lead to an emergent *odd in momentum* SOC in the conduction band. A combination of these effects typically results in a topologically non-trivial superfluid state in a number-conserving system with potential emergence of Majorana modes. We illustrated the above mechanism by studying a system of spinless fermions in a quasi-1D lattice with a dimerized structure and showed how one can observe this physics in a quantum simulator with alkaline-earth atoms with a variety of probes, including momentum-resolved spectroscopy and an analog of the spin-galvanic effect, i.e. a magneto-electric phenomenon that can be used to detect superfluidity with broken inversion symmetry.

In order to observe the TSF in cold-atom experiments, one needs to reach temperatures below the critical value T_c. In section 2.1 we estimated $T_c \sim 0.1 J_g$ when $u_{gg} \sim J_g$. Assuming $J_g \sim 100$ Hz (controlled by the g-atom lattice depth), $T_c \sim 10$ Hz ~ 0.5 nK. Because $u_{gg} = (U_{eg}^-)^2/4J_e$, reaching the condition $u_{gg} \sim J_g$ will be possible when $J_e \sim 1$ kHz [22] and $U_{eg}^- = 2\sqrt{u_{gg}J_e} \sim 600$Hz. The latter values are compatible with $J_g \sim 100$ Hz if the e-atoms are loaded in a higher lattice band of the double-well superlattice (in order to satisfy $|J_e| > |J_g|$) and if one takes advantage of the tighter confinement from the zero-magic lattice experienced only by the e-atoms.

While achieving such low temperatures is non-trivial, they are still feasible under current experimental capabilities, in particular given that it is the entropy (and not the actual temperature) what matters for cold-atom experiments. We note that if one can follow the preparation protocol discussed in section 3, it might be possible to adiabatically create the superfluid phase by preparing a high-fidelity band insulator as a starting point. Indeed, assuming that step (5) in figure 4 is adiabatic, $J_g = 100$ Hz and temperature $T = 0.5T_c = 5$ Hz, the required entropy is $S \approx 0.05 k_B$ per (nuclear-spin polarized) atom, which is achievable in current experiments [63]. Moreover, in alkaline-earth atoms the fidelity of the band insulator can be further increased by using the large number of nuclear-spin degrees of freedom. The enlarged Hilbert space should allow for more efficient sympathetic cooling [64–68]. This improved condition, when followed up by an appropriate filtering protocol to isolate a single nuclear spin component without heating the gas, could help to reduce the initial entropy of the cloud before loading it in the lattice. The individual addressing capabilities offered by optical tweezers might further help with the preparation of desired low-entropy initial band insulator.

In section 3, we assumed that our preparation protocol does not introduce random defects into the system, for instance, e-holes, i.e. empty double-wells without e-atoms. Despite the quasi-1D nature of our setup, this disorder will not necessarily lead to complete Anderson localization of single-particle states due to the strong SOC inherent to our system [69]. Moreover, because of the p-wave nature of our TSF state, it is expected to be robust against moderate disorder [70] when the mean-free path is larger than the superfluid coherence length. As the disorder strength is increased, potentially localized zero-modes will become gapped and the topological state is destroyed. However, one should remember that a significant density of e-holes will also suppress g-atom pairing, so the superfluid state is likely to be destroyed even before the above topological transition occurs. We leave detailed investigation of this issue for a future work.

The analysis presented in the main text can be easily extended beyond quasi-1D. One way to accomplish this was already described in section 2.1 (i.e. adding transverse g-atom nearest-neighbor hopping $J_g^\perp$). Another route is to prepare a 2D system where g-atoms propagate in a square lattice, and e-atoms are localized inside square plaquettes. In this case, similar arguments show that quantum fluctuations of the e-atoms stabilize a $p_x + i\,p_y$ superfluid state of the g-species (see appendix G).

Acknowledgments

We thank Daniel Agterberg, Victor Gurarie, Colin Kennedy, Johannes Schachenmayer, Dmitry Solenov, and Ilya Vekhter for illuminating discussions. This work was supported by NSF (PHY-1820885, PHY-1521080 and

JILA-PFC-PHY-1734006), AFOSR FA9550-18-1-0319, AFOSR-MURI Advanced Quantum Materials, NIST and W911NF-19-1-0210 through ARO.

Appendix A. Derivation of the *g*-atom effective Hamiltonian (2)

We focus on the regime $J_e \gg J_g, U_{eg}^-$ when the interaction term $\hat{H}_{\rm int} = U_{eg}^- \sum_{ia} \hat{n}_{ia}^g \hat{n}_{ia}^e$ and *g*-atom kinetic energy $\hat{H}_0^g$ in equation (1) can be treated as a small correction to the kinetic energy of *e*-atoms $\hat{H}_0^e = -J_e \sum_i (\hat{e}_{i1}^\dagger \hat{e}_{i2} + \text{h.c.})$, and use perturbation theory to compute the effective low-energy model (2). The zero-order subspace is spanned by the states $|\Psi_{eg}\rangle = \prod_i |\lambda\rangle_i \otimes |\Psi_g\rangle$. Because $J_g \ll J_e$, we consider this subspace degenerate for all $|\Psi_g\rangle$. To determine 1st (2nd) order corrections to the wavefunctions (energy eigenvalues), we employ the Schrieffer–Wolff transformation (SWT) method which systematically removes *off-diagonal* matrix elements of $\hat{H}_{\rm int}$ between states $|\Psi_{eg}\rangle$ to each order in U_{eg}^- [71]: $\hat{H} = \hat{H}_0^e + \hat{H}_{\rm int} \to e^{\hat{S}} \hat{H} e^{-\hat{S}}$ with $\hat{S} = \hat{S}_1 + \hat{S}_2 + \ldots$ being an anti-hermitian generator of the SWT and $\hat{S}_n \sim (U_{eg}^-)^n$. Notice that $\hat{H}_0^g$ acts only on the *g*-atom states $|\Psi_g\rangle$ and contains only *diagonal* matrix elements, thus representing a 1st order correction. On the other hand, $\hat{H}_{\rm int}$ has both off-diagonal and diagonal elements. The latter are proportional to $\sum_{ia} \hat{n}_{ia}^g$, i.e. they only correct the *g*-atom chemical potential and can be omitted.

To the first order in U_{eg}^-, $\hat{S}$ is given by:

$$\hat{S}_1 \;=\; U_{eg}^- \sum_{ia, E_e' E_e} \frac{\hat{P}_{E_e'}\, \widetilde{\hat{n}}^e_{ia}\, \hat{P}_{E_e}}{E_e' - E_e}\, \hat{n}_{ia}^g,$$

where $\hat{P}_{E_e}$ is the projector onto the state $\prod_i |\lambda\rangle_i$ of the *e*-subsystem with an energy E_e, and $\widetilde{\hat{n}}^e_{ia}$ is an off-diagonal part of the matrix ${}_i\langle\lambda'|\hat{n}^e_{ia}|\lambda\rangle_i = \frac{1}{2}\delta_{\lambda'\lambda} + \frac{1}{2}\sigma^x_{\lambda'\lambda}(\delta_{a1} - \delta_{a2})$ (δ_{ab} is a Kronecker delta-symbol).

The generator $\hat{S}_1$ yields a 2nd order in U_{eg}^- correction $\hat{H}_2 = \frac{1}{2}[\hat{S}_1, \hat{H}_{\rm int}]$ which operates in the degenerate manifold $\{|\Psi_{eg}\rangle\}$:

$$\begin{aligned} \hat{H}_2 &= \frac{(U_{eg}^-)^2}{2} \sum_{\substack{iab \\ E_e' E_e}} {}_i\!\left\langle \lambda \,\middle|\, \frac{\hat{P}_{E_e'}\, \widetilde{\hat{n}}^e_{ia}\, \hat{P}_{E_e}}{E_e' - E_e} \widetilde{\hat{n}}^e_{ib} \,\middle|\, \lambda \right\rangle_i \hat{n}_{ia}^g \hat{n}_{ib}^g + \text{h.c.} \\ &= \lambda u_{gg} \sum_i \hat{n}_{i1}^g \hat{n}_{i2}^g \end{aligned} \tag{A1}$$

with $u_{gg} = (U_{eg}^-)^2/4J_e$ and $\lambda = \pm 1$. The *g*-atom interaction can be controlled by preparing the *e*-subsystem in a particular local state: it is repulsive (attractive) for a (anti-) symmetric *e*-state $\lambda = +1$ ($\lambda = -1$).

The above calculation can be straightforwardly generalized to the case of a finite *e*-atom hopping between dimers, $\delta_e J_e \ll J_e$, when the levels at $\pm J_e$ become narrow bands with dispersion $\epsilon^e_{k\lambda} = -\lambda J_e |1 + \delta_e e^{ik}| = -\lambda \epsilon^e_k$ and the zero-order subspace is described by $|\Psi_{eg}\rangle = \prod_k |\lambda_k\rangle \otimes |\Psi_g\rangle$. Here the *e*-atom eigenstates are $|\lambda_k\rangle = \frac{1}{\sqrt{2}}(\hat{e}_{k1}^\dagger + \lambda e^{-i\varphi_k} \hat{e}_{k2}^\dagger)|\text{vac}\rangle$ with $\tan\varphi_k = \delta_e \sin k/(1 + \delta_e \cos k)$. The product in $|\Psi_{eg}\rangle$ runs over all *k*-states in a single λ-band, reflecting the unit filling of *e*-atoms.

To compute the perturbative effect of $\hat{H}_{\rm int}$, we again employ the SWT similar to the one described above. However, because *e*-atoms are now delocalized, the 2nd order correction $\hat{H}_2$ will describe non-local interactions of *g*-atoms on different dimers, similar to the RKKY interaction of magnetic moments in metals [72]. A simple calculation yields:

$$\begin{aligned} \hat{H}_2^{\rm RKKY} = -\lambda \left(\frac{U_{eg}^-}{2N_d}\right)^2 \sum_{k'k\, ij} \frac{e^{i(k'-k)(x_i - x_j)}}{\epsilon^e_{k'} + \epsilon^e_k} \\ \times (\hat{n}_{i1}^g - \hat{n}_{i2}^g e^{i(\varphi_{k'} - \varphi_k)})(\hat{n}_{j1}^g - \hat{n}_{j2}^g e^{-i(\varphi_{k'} - \varphi_k)}). \end{aligned}$$

In this expression, the denominator contains '+' sign because for the unit *e*-atom filling, only inter-band transitions (that change λ) are allowed and $\epsilon^e_{k\lambda} \sim \lambda$. Clearly, for $\delta_e = 0$ when $\epsilon^e_{k'} = \epsilon^e_k = J_e$ and $\varphi_k = 0$, $\hat{H}_2^{\rm RKKY}$ reduces to equation (A1).

A detailed investigation of the phases generated by $\hat{H}_2^{\rm RKKY}$ is beyond the scope of the present work. Here we only mention that for $\delta_e \ll 1$, corrections to the local model (A1) appear starting from 2nd order in δ_e: $\hat{H}_2^{\rm RKKY} = \hat{H}_2 + \mathcal{O}(\delta_e^2)$. Indeed, 1st order corrections to the summand will have the form $\delta_e(l_k + l_{k'})$, where l_k is some linear combination of $\sin k$ and $\cos k$. Because $\left(\frac{1}{N_d}\right)^2 \sum_{k'k} e^{i(k'-k)z} l_k \sim \delta_{z,0}\delta_{z,\pm 1} = 0$, there are no linear in δ_e terms in the perturbative expansion of $\hat{H}_2^{\rm RKKY}$.

Appendix B. BCS theory in a translationally invariant 1D system

In this section, we present a simple BCS theory that can be treated analytically and a number of insights can be gained on the structure of the topological SF phase. In particular, we analyze the singlet-triplet mixing of Cooper pair states due to the SOC in equation (2).

At the BCS level [73], the linearized interaction $\hat{H}_{\rm int}$ in (2) becomes:

$$\hat{H}_{\rm int} \approx \sum_k [\Delta\, \hat{g}^\dagger_{k1}\hat{g}^\dagger_{-k,2} + \text{h.c.}],$$

where $\Delta = -\frac{u_{gg}}{N_d}\sum_k \langle \hat{g}_{-k,2}\hat{g}_{k1}\rangle \equiv -\mathrm{i}\Delta_0 \mathrm{e}^{\mathrm{i}\phi_\Delta}$ (real Δ_0) is an s-wave OP. Because the above interaction couples fermions with opposite momenta, to avoid overcounting of k-states we will restrict momentum summations to a 'positive' half of the BZ with $k > 0$ (indicated by a prime), and denote $\hat{g}_{-k,a} \equiv \hat{G}_{ka}$ ($-k$ belongs to the other half of the BZ): $\sum_k f(\hat{g}_{ka}, \hat{g}_{-k,b}) = \sum'_k [f(\hat{g}_{ka}, \hat{G}_{kb}) + f(\hat{G}_{ka}, \hat{g}_{kb})]$. Then

$$\begin{aligned}\hat{H}_{\rm int} &\approx \sum_k{}' [\Delta\, (\hat{g}^\dagger_{k1}\hat{G}^\dagger_{k2} + \hat{G}^\dagger_{k1}\hat{g}^\dagger_{k2}) + \text{h.c.}] \\ &= \Delta_0\sigma^y_{ab}\sum_k{}' [\mathrm{e}^{\mathrm{i}\phi_\Delta}\hat{g}^\dagger_{ka}\hat{G}^\dagger_{kb} - \text{h.c.}].\end{aligned}$$

Similarly, the kinetic energy in equation (2) can be written as

$$\hat{H}^g_0 = \sum_k \epsilon_{ab}(k)\hat{g}^\dagger_{ka}\hat{g}_{kb} = \sum_k{}' \epsilon_{ab}(k)[\hat{g}^\dagger_{ka}\hat{g}_{kb} - \hat{G}_{ka}\hat{G}^\dagger_{kb}]$$

because $\epsilon(k) = -J_g[(1+\cos k)\sigma^x + \sin k\, \sigma^y] = \epsilon^T(-k)$.

Up to constant terms, the full BCS Hamiltonian is

$$\hat{H}_{\rm BCS} = \sum_k{}' (\hat{g}^\dagger_{ka}\ \hat{G}_{ka}) \underbrace{\begin{pmatrix} \epsilon_{ab} - \mu\delta_{ab} & \Delta_0\mathrm{e}^{\mathrm{i}\phi_\Delta}\sigma^y_{ab} \\ \Delta_0\mathrm{e}^{-\mathrm{i}\phi_\Delta}\sigma^y_{ab} & \mu\delta_{ab} - \epsilon_{ab}\end{pmatrix}}_{\mathcal{H}_{\rm BdG}} \begin{pmatrix}\hat{g}_{k,b} \\ \hat{G}^\dagger_{k,b}\end{pmatrix}.$$

The BdG Hamiltonian $\mathcal{H}_{\rm BdG}$ can be easily diagonalized when the OP Δ is purely imaginary. This scenario is still quite general, and below we will focus on the case $\phi_\Delta = 0$ when $\mathcal{H}_{\rm BdG} = (\sigma^z \otimes [\epsilon - \mu]) + \Delta_0(\sigma^x \otimes \sigma^y)$. It is diagonalized by performing a unitary transformation $\mathcal{H}_{\rm BdG} \to \mathcal{H}^y_{\rm BdG} = (U^\dagger \otimes 1)\mathcal{H}_{\rm BdG}(U \otimes 1)$ with $U = \frac{1}{\sqrt{2}}\begin{pmatrix}1 & 1 \\ \mathrm{i} & -\mathrm{i}\end{pmatrix}$. The eigenstates $\psi_{\nu\tau}$ are labeled by two indices τ and $\nu = \pm 1$, and have the form

$$\psi_{\nu\tau} = \frac{1}{2T_{k\tau}}\begin{pmatrix}[\nu T_{k\tau} + h_k]u_{k\tau} \\ \mathrm{i}[\nu T_{k\tau} - h_k]u_{k\tau}\end{pmatrix} \tag{B1}$$

with $h_k = \epsilon(k) - \mu + \mathrm{i}\Delta_0\sigma^y$ and the spinor

$$u_{k\tau} = \frac{1}{\sqrt{2R_k(R_k + \tau D_k)}}\begin{pmatrix}R_k + \tau D_k \\ \tau\mu(1 + \mathrm{e}^{\mathrm{i}k})\end{pmatrix}.$$

The corresponding energies are $E_{k\nu\tau} = \nu T_{k\tau}$ with $T_{k\tau} = \sqrt{\mu^2 + \Delta_0^2 + 2J_g^2(1+\cos k) + 2\tau J_g R_k}$, $R_k = \sqrt{D_k^2 + 2\mu^2(1+\cos k)}$ and $D_k = \Delta_0(1+\cos k)$.

The parameter Δ_0 is determined from the BCS self-consistency condition:

$$\begin{aligned}\Delta_0 &= -\frac{u_{gg}}{N_d}\sum_k{}' \sigma^y_{ab}\langle \hat{g}_{k,a}\hat{G}_{k,b}\rangle \\ &= \frac{\Delta_0 u_{gg}}{4N_d}\sum_{k\tau}\frac{\mathrm{th}\,\frac{\beta T_{k\tau}}{2}}{T_{k\tau}}\left[1 + \tau\frac{J_g}{R_k}(1+\cos k)^2\right]\end{aligned}$$

with the inverse temperature $\beta = 1/T$. To solve this equation, let us assume that the Fermi level (corresponding to momentum $k_{\rm F}$) lies below zero, i.e. $\mu = -J_g\sqrt{2(1+\cos k_{\rm F})} < 0$. Near the Fermi level $\delta k = |k| - k_{\rm F}$, $T_{k,+1} = 2|\mu|$ and $T_{k,-1} = \sqrt{\Delta_0^2 + v_F^2\delta k^2}$, with Fermi velocity $v_F = J_g\sqrt{1 - (\mu/2J_g)^2}$. In the weak coupling and zero-temperature limits, the main contribution to the sum comes from around the Fermi surface:

$$\begin{aligned}1 \approx \frac{u_{gg}}{4N_d}\sum_k{}' \frac{1}{T_{k,-1}}\left[1 - \frac{J_g}{R_k}(1+\cos k)^2\right]_{k=k_{\rm F}} &= \frac{u_{gg}}{4}\frac{2}{2\pi} \\ \times \int_0^{\lesssim k_{\rm F}} \frac{\mathrm{d}k}{\sqrt{\Delta_0^2 + v_F^2\delta k^2}}\frac{v_F^2}{J_g^2} &= \frac{u_{gg}}{2\pi J_g}\sqrt{1 - \frac{\mu^2}{(2J_g)^2}}\ln\frac{2\rho}{\Delta_0}.\end{aligned}$$

From here, $\Delta_0 = 2\rho e^{-2\pi J_g/u_{gg}\sqrt{1-(\mu/2J_g)^2}}$ with $\rho \sim J_g \gg \Delta_0$—a characteristic energy measured from the Fermi level beyond which the above expansion becomes invalid.

The OP Δ_0 involves g-fermions with opposite pseudospin a and describes an s-wave Cooper pairing. However, due to the SOC inherent in $\hat{H}_0^g$, there is also an admixture of the p-wave pairing states of two g-atoms with the same pseudospin which, because of Fermi statistics, must be antisymmetric in momentum. To quantify these p-wave correlations, we compute a spin-averaged pairing amplitude $\mathcal{P} = \frac{1}{2\Delta_0}\sum_a \langle \hat{g}_{ka}\hat{G}_{ka}\rangle$ using the BdG wavefunctions (B1):

$$\mathcal{P} = \frac{\mu \sin k}{4R_k}\sum_\tau \frac{\tau}{T_{k\tau}}\mathrm{th}\,\frac{\beta T_{k\tau}}{2}.$$

This result demonstrates that p-wave correlations in the system are enslaved to the s-wave OP. Moreover, the τ-dependence of the quasiparticle energy is essential: if $T_{k,+1} = T_{k,-1}$, as it would be in the absence of SOC, there is no p-wave pairing and $\mathcal{P} \equiv 0$.

Finally, we derive the BCS approximation in the weak-coupling limit described by equation (3). Introducing the pairing OP $\Delta = -\frac{u_{gg}}{4N_d}\sum_k e^{-i\frac{k}{2}}\langle \hat{f}_{-k}\hat{f}_k\rangle$, one can linearize the Hamiltonian (3):

$$\begin{aligned}\hat{H}_{\mathrm{ef}} &\approx \sum_k [(\epsilon_k - \mu)\hat{f}_k^\dagger \hat{f}_k + \Delta e^{i\frac{k}{2}}\hat{f}_k^\dagger \hat{f}_{-k}^\dagger + \mathrm{h.c.}] \\ &= \sum_k{}' \left[(\epsilon_k - \mu) + \begin{pmatrix}\hat{f}_k^\dagger & \hat{F}_k\end{pmatrix}\begin{pmatrix}\epsilon_k - \mu & D_k \\ D_k^* & \mu - \epsilon_k\end{pmatrix}\begin{pmatrix}\hat{f}_k \\ \hat{F}_k^\dagger\end{pmatrix}\right],\end{aligned} \tag{B2}$$

where $D_k = 2i\Delta \sin\frac{k}{2}$, $\epsilon_{-k} = \epsilon_k$, as before $\sum_k'\ldots$ extends over half of the BZ, and $\hat{F}_k = \hat{f}_{-k}$. This Hamiltonian is diagonalized by a Bogoliubov transformation from f-fermions to quasiparticles $\hat{\gamma}_k$ and $\hat{\Gamma}_k$ [1]:

$$\begin{aligned}\begin{pmatrix}\hat{f}_k \\ \hat{F}_k^\dagger\end{pmatrix} = \frac{1}{\sqrt{2E_k}}\Bigg[&\frac{1}{\sqrt{E_k + (\epsilon_k - \mu)}}\begin{pmatrix}E_k + (\epsilon_k - \mu) \\ D_k^*\end{pmatrix}\hat{\gamma}_k \\ &- \frac{1}{\sqrt{E_k - (\epsilon_k - \mu)}}\begin{pmatrix}E_k - (\epsilon_k - \mu) \\ -D_k^*\end{pmatrix}\hat{\Gamma}_k^\dagger\Bigg].\end{aligned} \tag{B3}$$

Here $E_k = \sqrt{(\epsilon_k - \mu)^2 + |D_k|^2}$ is the quasiparticle dispersion. The SF gap has a p-wave symmetry: $D_k = -D_{-k}$ and its amplitude Δ is determined from the self-consistency equation $1 = \frac{u_{gg}}{4N_d}\sum_k \sin^2\frac{k}{2}\Big/E_k$: $\Delta \sim e^{-2\pi J_g/u_{gg}\sqrt{1-(\mu/2J_g)^2}}$, which coincides with the result obtained in the multi-band case.

Appendix C. Unconstrained HFB theory in position space

In the present section, we summarize the fully unconstrained HFB mean-field approach [74] which we used to compute the phase diagram in figure 2. This variational technique treats on an equal footing SF and normal phases, including various insulating states that break translational symmetry, and hence provides an additional check of robustness of the TSF phase. Our method amounts to the following linearization of the four-fermion interaction:

$$\begin{aligned}\hat{H}_{\mathrm{int}} &= -u_{gg}\sum_i \hat{g}_{i1}^\dagger \hat{g}_{i2}^\dagger \hat{g}_{i2}\hat{g}_{i1} \approx -u_{gg}\sum_i [\hat{h}_{\mathrm{H}} + \hat{h}_{\mathrm{F}} + \hat{h}_B]; \\ \hat{h}_{\mathrm{H}} &= \langle \hat{n}_{i1}^g\rangle \hat{g}_{i2}^\dagger \hat{g}_{i2} + \langle \hat{n}_{i2}^g\rangle \hat{g}_{i1}^\dagger \hat{g}_{i1}; \\ \hat{h}_{\mathrm{F}} &= -\langle \hat{g}_{i1}^\dagger \hat{g}_{i2}\rangle \hat{g}_{i2}^\dagger \hat{g}_{i1} - \mathrm{h.c.} = \xi_i \hat{g}_{i1}^\dagger \hat{g}_{i2} + \mathrm{h.c.}; \\ \hat{h}_{\mathrm{B}} &= \langle \hat{g}_{i2}\hat{g}_{i1}\rangle \hat{g}_{i1}^\dagger \hat{g}_{i2}^\dagger + \mathrm{h.c.} = -\frac{\Delta_i}{u_{gg}}\hat{g}_{i1}^\dagger \hat{g}_{i2}^\dagger - \mathrm{h.c.},\end{aligned} \tag{C1}$$

where $\hat{h}_{\mathrm{H,F,B}}$ refer to Hartree, Fock and Bogoliubov contributions with (in general complex) OPs $n_{ia}^g = \langle \hat{g}_{ia}^\dagger \hat{g}_{ia}\rangle$, $\xi_i = -\langle \hat{g}_{i2}^\dagger \hat{g}_{i1}\rangle$, and $\Delta_i = -u_{gg}\langle \hat{g}_{i2}\hat{g}_{i1}\rangle$. The full HFB mean-field Hamiltonian includes $\hat{H}_{\mathrm{int}}$ and the g-atom kinetic energy $\hat{H}_0^g$ (see equation (2)), and can be written as:

$$\hat{H}_{\mathrm{HFB}} = \frac{1}{2}\sum_{\alpha\beta}\begin{pmatrix}\hat{g}_\alpha^\dagger & \hat{g}_\alpha\end{pmatrix}\underbrace{\begin{pmatrix}X_{\alpha\beta} & D_{\alpha\beta} \\ -D_{\alpha\beta}^* & -X_{\alpha\beta}^*\end{pmatrix}}_{\mathcal{H}_{\alpha\beta}}\begin{pmatrix}\hat{g}_\beta \\ \hat{g}_\beta^\dagger\end{pmatrix}$$

with composite indices $\alpha = \{ia\}$ and $\beta = \{jb\}$, and $2N_d \times 2N_d$ dimensional matrices $D_{\alpha\beta} = \mathrm{i}\sigma^y_{\alpha\beta}\Delta_i\delta_{ij}$ and

$$X_{\alpha\beta} = X_{ia,jb} = -J_g[\delta_{ij}\sigma^x_{ab} + (\delta^{b1}_{a2}\delta_{j,i+1} + \delta^{b2}_{a1}\delta_{j,i-1})] - \mu\delta_{ij}\delta_{ab} - u_{gg}\delta_{ij}\begin{pmatrix} n^g_{i2} & \xi_i \\ \xi^*_i & n^g_{i1}\end{pmatrix}_{ab}.$$

The kernel $\mathcal{H}_{\alpha\beta}$ has the property $\tau^x\mathcal{H}^*\tau^x = -\mathcal{H}$ with $\tau^x = (\sigma^x \otimes \delta_{\alpha\beta})$, which guarantees that its spectrum is even with respect to zero energy. We shall enumerate its positive eigenvalues by $\nu = 1, \ldots, n_\nu$ with $n_\nu = 2N_d$. $\hat{H}_{\mathrm{HFB}}$ can be diagonalized by a Bogoliubov transformation

$$\begin{pmatrix}\hat{g}_\alpha \\ \hat{g}^\dagger_\alpha\end{pmatrix} = \sum_\nu^{n_\nu}[\psi^\nu\hat{\gamma}_\nu + (\tau^x\psi^\nu)^*\hat{\gamma}^\dagger_\nu],$$

where $\hat{\gamma}_\nu$ are new fermionic modes and ψ^ν is an eigenstate of $\mathcal{H}$ corresponding to an energy $E_\nu \geqslant 0$. These states obey a completeness relation $\sum_\nu^{n_\nu}[\psi^{*\nu}_p\psi^\nu_q + (\tau^x\psi^\nu)_p(\tau^x\psi^\nu)^*_q] = \delta_{pq}$ with p and $q = 1, \ldots, 4N_d$.

Using the above quasiparticle modes, we can write down the self-consistency relations:

$$\Delta_i = -\frac{u_{gg}}{2}\sum\nolimits_\nu^{n_\nu}[\psi^{*\nu}_{(i1)+2N_d}\psi^\nu_{(i2)} - \psi^{*\nu}_{(i2)+2N_d}\psi^\nu_{(i1)}]\phi_\nu,$$
$$n^g_{ia} = \frac{1}{2} - \frac{1}{2}\sum\nolimits_\nu^{n_\nu}[|\psi^\nu_{(ia)}|^2 - |\psi^\nu_{(ia)+2N_d}|^2]\phi_\nu,$$
$$\xi_i = \frac{1}{2}\sum\nolimits_\nu^{n_\nu}[\psi^{*\nu}_{(i2)}\psi^\nu_{(i1)} - \psi^{*\nu}_{(i1)+2N_d}\psi^\nu_{(i2)+2N_d}]\phi_\nu,$$

where $\phi_\nu = 1 - 2f_\nu$ and $f_\nu = \langle\hat{\gamma}^\dagger_\nu\hat{\gamma}_\nu\rangle = 1/(\mathrm{e}^{E_\nu/T} + 1)$.

The quantum phase diagram (figure 2) was computed by minimizing the grand potential $\mathcal{G} = \langle\hat{H}_{\mathrm{HFB}}\rangle$ (notice, $\hat{H}_{\mathrm{HFB}}$ already includes the term $-\mu\sum_{ia}\hat{n}^g_{ia}$):

$$\frac{\mathcal{G}}{N_d} = -\mu - \frac{1}{N_d}\sum_i\left[\frac{|\Delta_i|^2}{u_{gg}} + u_{gg}(n^g_{i1}n^g_{i2} - |\xi_i|^2)\right] - \frac{1}{2N_d}\sum_{\alpha\beta}X_{\alpha\beta}(u_{gg}=0)\sum_\nu^{n_\nu}[\psi^{*\nu}_\alpha\psi^\nu_\beta - \psi^{*\nu}_{\beta+2N_d}\psi^\nu_{\alpha+2N_d}].$$

Appendix D. Probing the *g*-atom attraction

Here we present a simple derivation of the time dependence of the number of doubly occupied dimers after the quench protocol described in the main text. Assume that the *g*–*g* interactions are Hubbard-like: $\hat{H}_{\mathrm{int}} = U\hat{V} = U\sum_i\hat{n}^g_{i1}\hat{n}^g_{i2}$, where U denotes the interaction strength whose sign is unknown and needs to be determined (in the main text, $U = -u_{gg} < 0$). The operator $\hat{V}$ is a projector onto states with only doubly-occupied dimers. Our task is to compute $n_2(t) = \langle\psi(t)|\hat{V}|\psi(t)\rangle$, where $|\psi(t)\rangle$ is the time-dependent state of the system.

At time $t = 0$ *g*-atoms fill the Fermi sea $|\psi_0\rangle = |\psi(t=0)\rangle = \prod_{k<k_F}\hat{f}^\dagger_{k,-1}|\mathrm{vac}\rangle$, where $|\mathrm{vac}\rangle$ is the vacuum state without particles and k_F is the Fermi momentum. The wavefunction at $t = t_0$ is $|\psi(t_0)\rangle = \mathrm{e}^{-\mathrm{i}\varphi\hat{V}}|\psi_0\rangle$ with $\varphi = Ut_0$, while for $t > t_0$ it is given by $|\psi(t > t_0)\rangle = \mathrm{e}^{-\mathrm{i}\hat{H}^g_0(t-t_0)}|\psi(t_0)\rangle$. Therefore,

$$n_2(t > t_0) = \langle\psi_0|\mathrm{e}^{\mathrm{i}\varphi\hat{V}}\mathrm{e}^{\mathrm{i}\hat{H}^g_0(t-t_0)}\hat{V}\mathrm{e}^{-\mathrm{i}\hat{H}^g_0(t-t_0)}\mathrm{e}^{-\mathrm{i}\varphi\hat{V}}|\psi_0\rangle.$$

Consider a short time $t_0 \ll 1/U$ when $\varphi \ll 1$ and $n_2(t) - \langle\psi_0|\hat{V}|\psi_0\rangle \approx \mathrm{i}\varphi\langle\psi_0|[\hat{V}, \mathrm{e}^{\mathrm{i}\hat{H}^g_0\tau}\hat{V}\mathrm{e}^{-\mathrm{i}\hat{H}^g_0\tau}]|\psi_0\rangle$. If in addition we limit ourselves to short-time dynamics, $\tau = t - t_0 \ll 1/J_g$, then $\mathrm{e}^{\mathrm{i}\hat{H}^g_0(t-t_0)}\hat{V}\mathrm{e}^{-\mathrm{i}\hat{H}^g_0(t-t_0)} \approx \hat{V} + \mathrm{i}(t-t_0)[\hat{H}^g_0, \hat{V}]$, and the final expression for $n_2(t)$ is:

$$n_2(t) = \langle\hat{V}\rangle + \varphi(t-t_0)\langle[\hat{V}, [\hat{V}, \hat{H}^g_0]]\rangle = \langle\hat{V}\rangle - \kappa\varphi(t-t_0).$$

Here $\langle\ldots\rangle = \langle\psi_0|\ldots|\psi_0\rangle$ and $\kappa = 2[\langle\hat{V}\hat{H}^g_0\hat{V}\rangle - E_0\langle\hat{V}^2\rangle]$ (E_0 is the GS energy). It is easy to see that $\kappa > 0$. Indeed, introducing a normalized wavefunction $|\psi^V_0\rangle = \hat{V}|\psi_0\rangle/\langle\hat{V}^2\rangle$, we have $\kappa = 2\langle\hat{V}^2\rangle[\langle\psi^V_0|\hat{H}^g_0|\psi^V_0\rangle - E_0]$, which is clearly positive.

Appendix E. Momentum-resolved spectroscopy signal

Here we derive the expression for $\mathcal{R}_\tau(\delta,\, k)$ used in the main text. Our approach almost exactly follows [24]. We use units such that $\hbar = k_B = 1$.

The transfer of g-atoms from the SF phase to e-states in an empty tube is governed by the operator:

$$\hat{V}_L = \Omega \sum_{ia} \hat{q}^\dagger_{ia}\hat{g}_{ia},$$

where Ω is the Rabi frequency and $\hat{q}^\dagger_{ia}$ creates an e-atom in well a of the ith dimer in the auxiliary (empty) tube. The initial state of the system contains N_g g-atoms, $|\psi_{\rm in}\rangle = |\psi^{i,g}_{N_g}\rangle \otimes |{\rm vac}\rangle$ ($|{\rm vac}\rangle$ is an empty state of the auxiliary tube). Its energy is $\mathcal{E}_{\rm in} = E^g_i + \mu N_g + \omega_0$, where ω_0 is the laser frequency (note that we work in the grand-canonical ensemble, so E^g_i already includes the chemical potential offset). In the final state, there is a single e-atom with momentum k and band index τ in the auxiliary tube: $|\psi_{\rm fi}\rangle = |\psi^{f,g}_{N_g-1}\rangle \otimes \hat{f}^\dagger_{k\tau}|{\rm vac}\rangle$ ($|\psi^{f,g}_{N_g-1}\rangle$ is an intermediate state of g-atoms with $N_g - 1$ particles). This state has an energy $\mathcal{E}_{\rm fi} = E^g_f + \mu(N_g - 1) + \nu_{eg} + \epsilon^e_{k\tau}$, where ν_{eg} is the e–g transition frequency ($\sim 10^{14}$ Hz for ^{87}Sr). Because ν_{eg} is a very large energy compared to SF energy scales, we introduce a laser detuning $\delta = \omega_0 - \nu_{eg}$. The operators $\hat{f}_{k\tau}$ are similar to the f-modes defined in the text: $\hat{f}_{k\tau} = \frac{1}{\sqrt{2}}\left[\hat{q}_{k1} - \frac{\tau}{r_k}(1 + \eta e^{ik})\hat{q}_{k2}\right]$. η parameterizes the e-atom band structure in the empty tube via $\epsilon^e_{k\tau} = \tau r_k = \tau\sqrt{1 + \eta^2 + 2\eta\cos k}$.

The transfer rate $\mathcal{R}$ can be computed with the aid of the Fermi golden rule [24]:

$$\mathcal{R}_\tau(\delta,\, k) = 2\pi \sum_{\rm in,fi} |\langle\psi_{\rm fi}|\hat{V}_L|\psi_{\rm in}\rangle|^2 \frac{e^{-E_{\rm in}/T}}{\mathcal{Z}}\delta(\mathcal{E}_{\rm fi} - \mathcal{E}_{\rm in}),$$

where summation is extended over all initial and final states, and $\mathcal{Z}$ is the grand partition function. The matrix elements of $\hat{V}$ are given by

$$\begin{aligned}\langle\psi_{\rm fi}|\hat{V}_L|\psi_{\rm in}\rangle &= \Omega\sum_{ka}\langle\psi^{f,g}_{N_g-1}|\hat{g}_{ka}|\psi^{i,g}_{N_g}\rangle\langle{\rm vac}|\hat{f}_{k\tau}\hat{q}^\dagger_{ka}|{\rm vac}\rangle \\ &= \frac{\Omega}{\sqrt{2}}\left[\langle f|\hat{g}_{k1}|i\rangle - \frac{\tau}{r_k}(1 + \eta e^{ik})\langle f|\hat{g}_{k2}|i\rangle\right],\end{aligned}$$

where $\langle f|\hat{g}_{ka}|i\rangle = \langle\psi^{f,g}_{N_g-1}|\hat{g}_{ka}|\psi^{i,g}_{N_g}\rangle$.

Using the single-particle spectral density [75],

$$\mathcal{A}_{ab}(\omega,\, k) = 2\pi\sum_{nm}\langle n|\hat{g}_{ka}|m\rangle\frac{e^{-E_m/T}}{\mathcal{Z}}\langle m|\hat{g}^\dagger_{kb}|n\rangle\,\delta(E_m - E_n - \omega),$$

we obtain after a straightforward calculation:

$$\mathcal{R}_\tau(\delta,\, k) = \frac{\Omega^2}{2}\left\{\mathrm{Tr}\,\mathcal{A}(\omega,\, k) - \frac{\tau}{r_k}[(1 + e^{ik})\mathcal{A}_{12}(\omega,\, k) + (1 + e^{-ik})\mathcal{A}_{21}(\omega,\, k)]\right\}$$

with $\omega = \epsilon^e_{k\tau} - \mu - \delta$. Noting that $\mathcal{A}_{21} = \mathcal{A}^*_{12}$, we arrive at the expression in the main text.

Appendix F. Magneto-electric phenomena

In this section we discuss novel magneto-electric effects that occur as a result of the *odd in momentum* SOC in the effective model (2) when it is subjected to a weak laser-induced synthetic magnetic field. We assume this field to be homogeneous: $\delta\hat{H}_{\rm ef} = -\boldsymbol{b}\cdot\sum_k \boldsymbol{\sigma}_{ab}\hat{g}^\dagger_{ka}\hat{g}_{kb}$. In particular, we shall derive weak-coupling expressions for the susceptibility χ and magneto-electric coefficient κ quoted in the main text.

It is well-known that a physical external magnetic field breaks time-reversal symmetry $\mathcal{T}$. However, because $\boldsymbol{b}$ is artificial, it does not necessarily break $\mathcal{T}$. Indeed, under time-reversal, the second-quantized operators and c-numbers transform as $\hat{g}_{ka} \to \hat{g}_{-k,a}$ (because a is not a real spin but the position index inside a dimer) and $c \to c^*$. Therefore, only the b_y-term in $\delta\hat{H}_{\rm ef}$ breaks $\mathcal{T}$ and is capable of generating a mass current. Below we focus on the case with $b_x = b_z = 0$ and $b_y \neq 0$ (see figure 7(a)).

It is instructive to study the non-interacting system described by the Hamiltonian $\hat{H}^g_0 + \delta\hat{H}_{\rm ef}$ [$\hat{H}^g_0$ is defined in equation (2)] which is diagonalized by Bogoliubov quasiparticles $\hat{f}_{k\tau} = \frac{1}{\sqrt{2}}\left[\hat{g}_{k1} - \frac{\tau}{R_k}(1 + e^{-ik} - i\, b_y)\hat{g}_{k2}\right]$ with energies $\epsilon_{k\tau} = \tau R_k = \tau\sqrt{2J^2_g(1 + \cos k) + b^2_y + 2J_g b_y \sin k}$. Assuming that $T = 0$ and f-particles fill the Fermi sea $|{\rm FS}\rangle$ with a chemical potential μ, i.e. $\langle{\rm FS}|\hat{f}^\dagger_{k\tau'}\hat{f}_{k\tau}|{\rm FS}\rangle = \delta_{\tau'\tau}\theta(\mu - \epsilon_{k\tau})$, the average mass current is (the operator $\hat{K}$ was defined in the main text)

$$\langle \mathrm{FS}|\hat{K}|\mathrm{FS}\rangle = \tfrac{2}{N_d}\sum_{k\tau}\tfrac{\tau}{R_k}(b_y\cos k - J_g\sin k)\langle \hat{f}^\dagger_{k\tau}\hat{f}_{k\tau}\rangle$$
$$= \tfrac{2}{J_g N_d}\sum_{k\tau}\frac{\partial\epsilon_{k\tau}}{\partial k}\,\theta(\mu-\epsilon_{k\tau}) = \tfrac{2}{J_g}(\mu-\mu) = 0.$$

This result is valid even in interacting non-SF systems. Hence a magnetic field cannot generate a mass current in the absence of SF correlations [27].

This situation changes dramatically when pairing correlations are taken into account, technically because the average current can no longer be written as an integral of the quasiparticle group velocity. Consider the weak-coupling dilute limit $u_{gg} \ll J_g$ and $n^g \ll 1$. In this regime, we can project interactions in equation (2) onto the lowest band $\tau = -1$. At small fields $b_y \ll J_g, \Delta$, the bare fermion operators become $\hat{g}_{k1} \approx \frac{1}{\sqrt{2}}\hat{f}_k$ and $\hat{g}_{k2} \approx \frac{1}{\sqrt{2}}e^{ik/2}(1 + ib_y/2J_g)\hat{f}_k$, where $\hat{f}_{k,-1} \equiv \hat{f}_k$. It is easy to check that b_y enters the projected interaction term in equation (2) only via quadratic corrections $\sim b_y^2$. Therefore, to linear order in b_y the projected Hamiltonian is the same as equation (3) with $\epsilon_k = -2J_g\cos\frac{k}{2} - b_y\sin\frac{k}{2} = \epsilon_k^{(0)} - b_y\sin\frac{k}{2}$. Since $-\epsilon_{-k} = -\epsilon_k^{(0)} - b_y\sin\frac{k}{2}$, the BdG Hamiltonian is

$$\mathcal{H}_{\mathrm{BdG}} = -b_y\sin\tfrac{k}{2} + \begin{pmatrix}\epsilon_k^{(0)} - \mu & D_k\\ D_k^* & \mu - \epsilon_k^{(0)}\end{pmatrix},$$

see equation (B2). The Bogoliubov transformation diagonalizing this Hamiltonian is given by (B3) with ϵ_k and E_k replaced by $\epsilon_k^{(0)}$ and $E_k^{(0)} = \sqrt{(\epsilon_k^{(0)} - \mu)^2 + |D_k|^2}$, respectively. However, energies of the quasiparticles $\hat{\gamma}_k$ and $\hat{\Gamma}_k$ are now split by a field correction and are given by $E_{k,\pm} = E_k^{(0)} \mp b_y\sin\frac{k}{2}$, respectively. If b_y is small, we can assume that sign $(E_{k,\pm}) = \pm$, and in the BCS GS $\langle\hat{\gamma}_k^\dagger\hat{\gamma}_k\rangle = \nu(E_{k,+})$ and $\langle\hat{\Gamma}_k^\dagger\hat{\Gamma}_k\rangle = \nu(E_{k,-})$ with the Fermi function $\nu(x) = (e^{x/T} + 1)^{-1}$.

The projected current and y-component of the pseudospin $\hat{S}_y$ have the form: $\hat{K} \approx \frac{1}{N_d}\sum_k\left(2\sin\frac{k}{2} - \frac{b_y}{J_g}\cos\frac{k}{2}\right)\hat{f}_k^\dagger\hat{f}_k$ and $\hat{S}_y = \frac{1}{2N_d}\sum_k\sigma^y_{ab}\hat{g}^\dagger_{ka}\hat{g}_{kb} \approx \frac{1}{4N_d}\sum_k\left(2\sin\frac{k}{2} + \frac{b_y}{J_g}\cos\frac{k}{2}\right)\hat{f}_k^\dagger\hat{f}_k$. In the BCS GS the first term in both expressions vanishes at $T = 0$ because $\sum_k'\sin\frac{k}{2}\langle\hat{f}_k^\dagger\hat{f}_k - \hat{F}_k^\dagger\hat{F}_k\rangle = \sum_k'\sin\frac{k}{2}[\nu(E_{k,+}) - \nu(E_{k,-})]$. Hence, $\kappa = \langle\hat{K}\rangle/b_y = -4\langle\hat{S}_y\rangle/b_y = -4\chi$. When $T = 0$, it is easy to show that κ is given by the expression in the main text. Figure 7(b) shows κ and χ numerically computed beyond the weak-coupling dilute limit. In the simulation we used the same strategy as above: solve the BdG equations in the field, compute $\langle\hat{K}\rangle$ and $\langle\hat{S}_y\rangle$ as functions of b_y, and extract the corresponding linear coefficients.

Appendix G. Topological superfluidity in a 2D lattice

The results presented in the main text, can be extended to higher dimensional systems. Here we briefly consider a generalization involving a lattice that has the plaquette structure shown in figure G1(a). In each plaquette, there is one e-atom that can tunnel around the plaquette (with lattice constant a_0). On the other hand, g-fermions move in the simpler square lattice. As before, all atoms are nuclear-spin-polarized and we use units where $a_0 = 1$. The Hamiltonian of this system is

$$\hat{H} = \hat{H}_0^e + \hat{H}_0^g + \hat{H}_{\mathrm{int}}; \tag{G1}$$
$$\hat{H}_0^e = -J_e\sum_{i,\square_{ab}}(\hat{e}^\dagger_{ia}\hat{e}_{ib} + \mathrm{h.c.});$$
$$\hat{H}_0^g = -J_g\Bigg[\sum_{i,\square_{ab}}(\hat{g}^\dagger_{ia}\hat{g}_{ib} + \mathrm{h.c.}) + \sum_{\langle ij\rangle_x}(\hat{g}^\dagger_{i2}\hat{g}_{j1} + \hat{g}^\dagger_{i3}\hat{g}_{j4}) + \sum_{\langle ij\rangle_y}(\hat{g}^\dagger_{i,4}\hat{g}_{j,1} + \hat{g}^\dagger_{i3}\hat{g}_{j2}) + \mathrm{h.c.}\Bigg];$$
$$\hat{H}_{\mathrm{int}} = U_{eg}^-\sum_{ia}\hat{n}^g_{ia}\hat{n}^e_{ia},$$

where $i = \boldsymbol{x}_i = (x_i, y_i)$, $i, j = 1, \ldots, N_\square$ label plaquettes in the lattice, $a, b = 1, 2, 3, 4$ denote wells inside a plaquette, $\square_{ab}$ indicates all sides $\langle ab\rangle$ of a square, and $\langle ij\rangle_{x,y}$ is a link connecting two plaquettes in the x or y direction (figure G1(a)). Other notations are the same as in equation (3).

In the rest of this section, we shall follow an analysis similar to the one in the main text: First, we consider e-atom states of an isolated plaquette and identify a spatial mode that gives rise to the g-atom attraction within that plaquette. Then, we study a weak-coupling dilute limit $u_{gg} \ll J_g, n^g \ll 1$ and demonstrate the stability of a

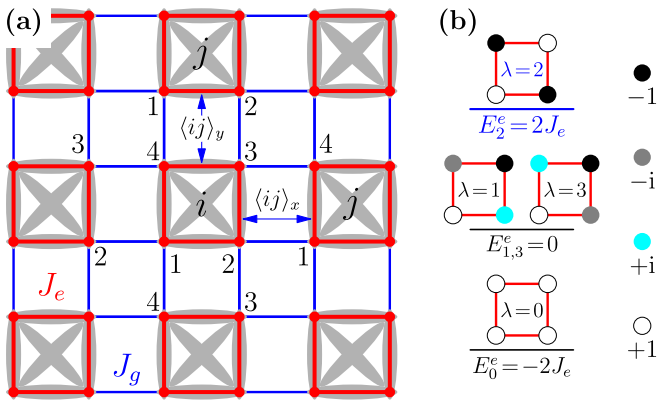

Figure G1. (a) Two-dimensional optical superlattice with a plaquette structure. The *e*-atoms are confined within red square plaquettes (with one atom per cell), *g*-atoms propagate in a simple square lattice (thin blue lines). Gray ellipses denote *g*-atom attraction mediated by fluctuations of the *e*-subsystem. Other notations are as in figure 1(a). (b) States of an *e*-atom within a plaquette. Also shown are point symmetries of the wavefunctions $X_a^{(\lambda)}=\frac{1}{2}e^{i\frac{\pi}{2}\lambda(a-1)}$ with colors indicating phases ±1 and $\pm i$. In particular, the $\lambda=0\,(2)$ state has *s*- (*d*-) wave symmetry. Attractive interactions between *g*-atoms occur when *e*-atoms are prepared in the $\lambda=2$ state.

chiral p_x+ip_y TSF state. The study of the phase diagram, magneto-electric effects, etc is left for a future investigation.

Pairing of the g-atoms.–An *e*-atom localized within a plaquette, has four states $\lambda=0,\ldots,3$ shown in figure G1(b). Their wavefunctions are $|\lambda\rangle_i=\sum_a X_a^{(\lambda)}\hat{e}_{ia}^\dagger|\text{vac}\rangle$ with $X_a^{(\lambda)}=\frac{1}{2}e^{i\frac{\pi}{2}\lambda(a-1)}$ and corresponding energies $E_0^e=-E_2^e=-2J_e$, $E_1^e=E_3^e=0$. Matrix elements of the density $\hat{n}_{ia}^e$ are ${}_i\langle\lambda'|\hat{n}_{ia}^e|\lambda\rangle_i=X_a^{(\lambda')*}X_a^{(\lambda)}=\frac{1}{4}e^{i\frac{\pi}{2}(\lambda-\lambda')(a-1)}$.

In the 1D case we saw that an attractive interaction between *g*-atoms occurs when the *e*-subsystem is prepared in the highest excited kinetic energy state. An analogous situation happens here: *e*-atoms must fluctuate out of the *d*-wave $\lambda=2$ state with energy $2J_e$. Using the Schrieffer–Wolff transformation, we obtain the second-order *g*-atom Hamiltonian

$$\hat{H}_{\text{ef}}=\hat{H}_0^g-u_{gg}\sum_i[(\hat{n}_{i1}^g+\hat{n}_{i3}^g)(\hat{n}_{i2}^g+\hat{n}_{i4}^g)+3(\hat{n}_{i1}^g\hat{n}_{i3}^g+\hat{n}_{i2}^g\hat{n}_{i4}^g)]. \tag{G2}$$

Here $u_{gg}=(U_{eg}^-)^2/32J_e$, and density terms in the 1st (2nd) line describe attractive interactions along sides (diagonals) of the *i*th plaquette (gray ellipses in figure G1(a)).

Weak-coupling dilute regime.–The *g*-atom kinetic energy can be written as

$$\hat{H}_0^g=-J_g\sum_{\boldsymbol{k}}\hat{g}_{ka}^\dagger\begin{pmatrix}0&\eta_{k_x}&0&\eta_{k_y}\\ \eta_{k_x}^*&0&\eta_{k_y}&0\\ 0&\eta_{k_y}^*&0&\eta_{k_x}^*\\ \eta_{k_y}^*&0&\eta_{k_x}&0\end{pmatrix}_{ab}\hat{g}_{kb},$$

where $\hat{g}_{ka}=\frac{1}{\sqrt{N_\square}}\sum_i e^{-i(\boldsymbol{k}\cdot\boldsymbol{x}_i)}\hat{g}_{ia}$, momentum $\boldsymbol{k}=(k_x,k_y)$ with $k_\alpha\in[-\pi,\pi]\,(\alpha=x,y)$ is defined in a plaquette BZ with $N_\square$ states and $\eta_{k_\alpha}=1+e^{-ik_\alpha}$. Eigenvalues of the matrix in $\hat{H}_0^g$ are $\pm2J_g\left[\cos\frac{k_x}{2}\pm\cos\frac{k_y}{2}\right]$. At weak coupling $u_{gg}\ll J_g$ and $n^g\ll1$, only the lowest band $\epsilon_{\boldsymbol{k}}=-2J_g\left[\cos\frac{k_x}{2}+\cos\frac{k_y}{2}\right]\approx-4J_g+\frac{k^2}{2m^*}$ is populated ($m^*=2/J_g$ is the effective mass). The corresponding eigenvector is $\psi_0=\frac{1}{2}(1,\,-e^{-i\varphi_x},\,e^{-i(\varphi_x+\varphi_y)},\,-e^{-i\varphi_y})^T$ with $e^{i\varphi_\alpha}=\eta_{k_\alpha}/|\eta_{k_\alpha}|$. At small momenta, $\psi_0\approx\frac{1}{2}(1,\,e^{ik_x/2},\,e^{i(k_x+k_y)/2},\,e^{ik_y/2})^T$.

The low-energy effective Hamiltonian can be obtained by replacing $\hat{g}_{\boldsymbol{k}}\to\psi_0 f_{\boldsymbol{k}}$ ($f_{\boldsymbol{k}}$ is the lowest-band fermion quasiparticle) in equation (G2):

$$\hat{H}_{\text{ef}}\approx\sum_{\boldsymbol{k}}\epsilon_{\boldsymbol{k}}\hat{f}_{\boldsymbol{k}}^\dagger\hat{f}_{\boldsymbol{k}}+\frac{u_{gg}}{16N_\square}\sum_{\boldsymbol{k}'\boldsymbol{k}\boldsymbol{q}}\boldsymbol{q}^2\hat{f}_{\boldsymbol{k}+\boldsymbol{q}}^\dagger\hat{f}_{\boldsymbol{k}'-\boldsymbol{q}}^\dagger\hat{f}_{\boldsymbol{k}'}\hat{f}_{\boldsymbol{k}}.$$

This expression describes a system of spinless fermions interacting via an attractive *p*-wave coupling. Within the BCS approximation we have:

$$\hat{H}_{\rm ef} \approx \sum_{k}\left[\xi_k \hat{f}_k^\dagger \hat{f}_k + \tfrac{1}{2}(\boldsymbol{k}\cdot\boldsymbol{\Delta})\hat{f}_k^\dagger \hat{f}_{-k}^\dagger + \text{h.c.}\right]$$
$$= \sum_{k}{}'\left[\xi_k + \begin{pmatrix}\hat{f}_k^\dagger & \hat{F}_k\end{pmatrix}\begin{pmatrix}\xi_k & D_k\\ D_k^* & -\xi_k\end{pmatrix}\begin{pmatrix}\hat{f}_k\\ \hat{F}_k^\dagger\end{pmatrix}\right].$$

Here we switched to a grand-canonical ensemble with a chemical potential μ and performed the standard replacement $\hat{H}_{\rm ef} \to \hat{H}_{\rm ef} - \mu\sum_{ia}\hat{n}_{ia}^g$. $\xi_k = \epsilon_k - \mu$, $D_k = (\boldsymbol{k}\cdot\boldsymbol{\Delta})$, and other notations are the same as in the 1D weak-coupling case. The above Hamiltonian is diagonalized by a Bogoliubov transformation identical to the one used in the 1D case after a replacement $k \to \boldsymbol{k}$. The pairing OP $\boldsymbol{\Delta} = -\frac{u_{gg}}{2N_\square}\sum_{\boldsymbol{k}}{}'\boldsymbol{k}\langle\hat{F}_k\hat{f}_k\rangle$ obeys the BCS equation

$$\boldsymbol{\Delta} = \frac{u_{gg}}{4N_\square}\sum_{k}{}'\frac{\boldsymbol{k}(\boldsymbol{k}\cdot\boldsymbol{\Delta})}{E_k} = \frac{u_{gg}}{8N_\square}\sum_{k}\frac{\boldsymbol{k}(\boldsymbol{k}\cdot\boldsymbol{\Delta})}{E_k}, \tag{G3}$$

where $E_k = \sqrt{\xi_k^2 + |D_k|^2}$ and in the last sum we used evenness of the integrand and extended summation over the entire BZ. Whenever the SF phase develops, the grand potential $\mathcal{G}_s$ in that phase is reduced compared to its normal-state value $\mathcal{G}_n$. This shift can be computed using the Hellman–Feynman theorem [1]

$$\frac{\delta\mathcal{G}}{N_\square} = \frac{\mathcal{G}_s - \mathcal{G}_n}{N_\square} = \int_0^{u_{gg}} \mathrm{d}\tilde{u}\,\frac{\langle\hat{H}_{\rm int}\rangle}{N_\square\,\tilde{u}} = -2\int_0^{u_{gg}}\mathrm{d}\tilde{u}\,\frac{|\Delta(\tilde{u})|^2}{\tilde{u}^2}.$$

There are two competing SF states characterized by different symmetries of the OP $\boldsymbol{\Delta}$: (i) chiral $p_x \pm \mathrm{i}p_y$ phase with $\boldsymbol{\Delta}_{p+\mathrm{i}p} = \Delta_1(\boldsymbol{e}_x^p \mp \mathrm{i}\boldsymbol{e}_y^p)$ ($\boldsymbol{p} = p_x\boldsymbol{e}_x^p + p_y\boldsymbol{e}_y^p$), and (ii) p_x (or p_y) state with $\boldsymbol{\Delta}_{p_x} = \Delta_2\boldsymbol{e}_x^p$ (or $\Delta_2\boldsymbol{e}_y^p$). Below we assume real amplitudes $\Delta_{1,2}$ and demonstrate that at weak coupling, the $p_x + \mathrm{i}p_y$ state is favored.

$p_x + \mathrm{i}p_y$ SF.–The u_{gg}-dependence of Δ_1 can be determined by multiplying equation (G3) by $\boldsymbol{\Delta}^*$ [notice that $|\boldsymbol{\Delta}|^2 = 2\Delta_1^2$ and $|\boldsymbol{k}\cdot\boldsymbol{\Delta}|^2 = \boldsymbol{k}^2\Delta_1^2$]: $2 = \frac{u_{gg}}{8N_\square}\sum_{\boldsymbol{k}}\frac{\boldsymbol{k}^2}{E_k} = \frac{u_{gg}}{16\pi}\int\mathrm{d}k\frac{k^3}{E_k} \approx \kappa\ln\frac{2\rho}{k_F\Delta_1}$, where $\kappa = u_{gg}Q_F$ with $Q_F \equiv \frac{m^*k_F^2}{8\pi}$, k_F is the Fermi momentum, and $\rho \sim J_g \gg \Delta_1$ is a characteristic energy cutoff. We have:

$$\frac{\delta\mathcal{G}_1}{N_\square} = 4Q_F\int_0^{\Delta_1}\mathrm{d}\left(\tfrac{1}{\kappa}\right)\Delta^2 = -Q_F\Delta_1^2 = -\frac{\rho^2 m^*}{2\pi}\mathrm{e}^{-4/\kappa}.$$

p_x SF.–Proceeding in a similar manner as above, we use the BCS equation (G3) to calculate Δ_2

$$1 = \frac{u_{gg}}{8N_\square}\sum_{k}\frac{k_x^2}{E_k} = \frac{u_{gg}}{8}\int\frac{\mathrm{d}k\,k}{2\pi}\oint\frac{d\theta}{2\pi}\frac{k^2\cos^2\theta}{\sqrt{\xi_k^2 + k^2\Delta_2^2\cos^2\theta}}$$
$$\approx \kappa\oint\frac{\mathrm{d}\theta}{2\pi}\cos^2\theta\ln\frac{2\rho}{k_F\Delta_2|\cos\theta|} = \frac{\kappa}{2}\left[\ln\frac{2\rho}{k_F\Delta_2} + I\right],$$

where $I = -2\oint\frac{\mathrm{d}\theta}{2\pi}\cos^2\theta\ln|\cos\theta| \approx 0.2$. $\delta\mathcal{G}$ can be computed as before

$$\frac{\delta\mathcal{G}_2}{N_\square} = 2Q_F\int_0^{\Delta_2}\mathrm{d}\left(\tfrac{1}{\kappa}\right)\Delta^2 = -\frac{Q_F\Delta_2^2}{2} = -\frac{\rho^2 m^*}{2\pi}\frac{\mathrm{e}^{2I}}{2}\mathrm{e}^{-4/\kappa}.$$

Because $\mathrm{e}^{2I}/2 < 1$, $\delta\mathcal{G}_1 < \delta\mathcal{G}_2$ and the $p_x \pm \mathrm{i}p_y$ SF state is preferred over the striped $p_{x,y}$ phase.

ORCID iDs

G Ortiz https://orcid.org/0000-0003-3254-4494

References

[1] Landau L, Lifshitz E and Pitaevskii L 1980 Course of theoretical physics No. pt. 2 *Statistical Physics* (Oxford : Pergamon Press)
[2] Qi X-L and Zhang S-C 2011 *Rev. Mod. Phys.* **83** 1057
[3] Nayak C, Simon S H, Stern A, Freedman M and Sarma S Das 2008 *Rev. Mod. Phys.* **80** 1083
[4] Ortiz G, Dukelsky J, Cobanera E, Esebbag C and Beenakker C 2014 *Phys. Rev. Lett.* **113** 267002
[5] Ortiz G and Cobanera E 2016 *Ann. Phys.* **372** 357
[6] Zeng B, Chen X, Zhou D-L and Wen X-G 2019 *Quantum Information Meets Quantum Matter; From Quantum Entanglement to Topological Phases of Many-Body Systems* (New York: Springer)
[7] Nussinov Z and Ortiz G 2009 *Proc. Natl Acad. Sci.* **106** 16944
[8] Volovik G 2009 International series of monographs on physics *The Universe in a Helium Droplet* (Oxford: Oxford University Press)
[9] Autti S, Dmitriev V V, Mäkinen J T, Soldatov A A, Volovik G E, Yudin A N, Zavjalov V V and Eltsov V B 2016 *Phys. Rev. Lett.* **117** 255301
[10] Read N and Green D 2000 *Phys. Rev.* B **61** 10267
[11] Botelho S S and Melo C A R S d 2005 *J. Low Temp. Phys.* **140** 409
[12] Rombouts S M A, Dukelsky J and Ortiz G 2010 *Phys. Rev.* B **82** 224510
[13] Bohn J L, Rey A M and Ye J 2017 *Science* **357** 1002

[14] Smidman M, Salamon M B, Yuan H Q and Agterberg D F 2017 *Rep. Prog. Phys.* **80** 036501
[15] Cazalilla M and Rey A 2014 *Rep. Prog. Phys.* **77** 124401
[16] Zhang X, Bishof M, Bromley S L, Kraus C V, Safronova M S, Zoller P, Rey A M and Ye J 2014 *Science* **345** 1467
[17] Cappellini G *et al* 2014 *Phys. Rev. Lett.* **113** 120402
[18] Scazza F, Hofrichter C, Höfer M, De Groot P C, Bloch I and Folling S 2014 *Nat. Phys.* **10** 779
[19] Sebby-Strabley J, Anderlini M, Jessen P S and Porto J V 2006 *Phys. Rev.* A **73** 033605
[20] Lee P J, Anderlini M, Brown B L, Sebby-Strabley J, Phillips W D and Porto J V 2007 *Phys. Rev. Lett.* **99** 020402
[21] Folling S, Trotzky S, Cheinet P, Feld M, Saers R, Widera A, Muller T and Bloch I 2007 *Nature* **448** 1029
[22] Trotzky S, Cheinet P, Fölling S, Feld M, Schnorrberger U, Rey A M, Polkovnikov A, Demler E A, Lukin M D and Bloch I 2008 *Science* **319** 295
[23] Stewart J T, Gaebler J P and Jin D S 2008 *Nature* **454** 744
[24] Dao T-L, Carusotto I and Georges A 2009 *Phys. Rev.* A **80** 023627
[25] Gor'kov L P and Rashba E I 2001 *Phys. Rev. Lett.* **87** 037004
[26] Yip S K 2002 *Phys. Rev.* B **65** 144508
[27] Ojanen T 2012 *Phys. Rev. Lett.* **109** 226804
[28] Goban A, Hutson R B, Marti G E, Campbell S L, Perlin M A, Julienne P S, D'Incao J P, Rey A M and Ye J 2018 *Nature* **563** 369
[29] Bishof M, Martin M J, Swallows M D, Benko C, Lin Y, Quéméner G, Rey A M and Ye J 2011 *Phys. Rev.* A **84** 052716
[30] Lemke N D, von Stecher J, Sherman J A, Rey A M, Oates C W and Ludlow A D 2011 *Phys. Rev. Lett.* **107** 103902
[31] Höfer M, Riegger L, Scazza F, Hofrichter C, Fernandes D R, Parish M M, Levinsen J, Bloch I and Fölling S 2015 *Phys. Rev. Lett.* **115** 265302
[32] Pagano G, Mancini M, Cappellini G, Livi L, Sias C, Catani J, Inguscio M and Fallani L 2015 *Phys. Rev. Lett.* **115** 265301
[33] Regal C A, Ticknor C, Bohn J L and Jin D S 2003 *Phys. Rev. Lett.* **90** 053201
[34] Zhang J, van Kempen E G M, Bourdel T, Khaykovich L, Cubizolles J, Chevy F, Teichmann M, Tarruell L, Kokkelmans S J J M F and Salomon C 2004 *Phys. Rev.* A **70** 030702
[35] Gaebler J P, Stewart J T, Bohn J L and Jin D S 2007 *Phys. Rev. Lett.* **98** 200403
[36] Chin C, Grimm R, Julienne P and Tiesinga E 2010 *Rev. Mod. Phys.* **82** 1225
[37] Galitski V and Spielman I B 2013 *Nature* **494** 49
[38] Goldman N, Juzeliunas G, Öhberg P and Spielman I B 2014 *Rep. Prog. Phys.* **77** 126401
[39] Celi A, Massignan P, Ruseckas J, Goldman N, Spielman I B, Juzelin¯as G and Lewenstein M 2014 *Phys. Rev. Lett.* **112** 043001
[40] Dalibard J, Gerbier F, Juzelin¯as G and Öhberg P 2011 *Rev. Mod. Phys.* **83** 1523
[41] Wang P, Yu Z-Q, Fu Z, Miao J, Huang L, Chai S, Zhai H and Zhang J 2012 *Phys. Rev. Lett.* **109** 095301
[42] Huang L, Meng Z, Wang P, Peng P, Zhang S-L, Chen L, Li D, Zhou Q and Zhang J 2016 *Nat. Phys.* **12** 540
[43] Cheuk L W, Sommer A T, Hadzibabic Z, Yefsah T, Bakr W S and Zwierlein M W 2012 *Phys. Rev. Lett.* **109** 095302
[44] Burdick N Q, Tang Y and Lev B L 2016 *Phys. Rev.* X **6** 031022
[45] Song B, He C, Zhang S, Hajiyev E, Huang W, Liu X-J and Jo G-B 2016 *Phys. Rev.* A **94** 061604
[46] Ye J, Kimble H J and Katori H 2008 *Science* **320** 1734
[47] Safronova M S, Zuhrianda Z, Safronova U I and Clark C 2015 *Phys. Rev.* A **92** 040501
[48] Eroles J, Ortiz G, Balatsky A V and Bishop A R 2000 *Europhys. Lett.* **50** 540
[49] Tsai W-F, Yao H, Läuchli A and Kivelson S A 2008 *Phys. Rev.* B **77** 214502
[50] Rey A M, Sensarma R, Folling S, Greiner M, Demler E and Lukin M D 2009 *Europhys. Lett.* **87** 60001
[51] Isaev L, Ortiz G and Batista C D 2010 *Phys. Rev. Lett.* **105** 187002
[52] Kitaev A Y 2001 *Phys.—Usp.* **44** 131
[53] Anderson P 1984 *Basic Notions of Condensed-Matter Physics* (Reading, MA : Addison-Wesley)
[54] Hu H, Jiang L, Liu X-J and Pu H 2011 *Phys. Rev. Lett.* **107** 195304
[55] Yu Z-Q and Zhai H 2011 *Phys. Rev. Lett.* **107** 195305
[56] Han L and Sá de Melo C A R 2012 *Phys. Rev.* A **85** 011606
[57] Kwon H-J, Sengupta K and Yakovenko V M 2004 *Eur. Phys. J* B **37** 349
[58] Wu K and Simon H 2000 *SIAM J. Matrix Anal. Appl.* **22** 602
[59] Kolkowitz S, Bromley S, Bothwell T, Wall M, Marti G, Koller A, Zhang X, Rey A and Ye J 2016 *Nature* **542** 66
[60] Anderson P W 1967 *Phys. Rev. Lett.* **18** 1049
[61] Bromley S L, Kolkowitz S, Bothwell T, Kedar D, Safavi-Naini A, Wall M L, Salomon C, Rey A and Ye J 2018 *Nat. Phys.* **14** 399
[62] Mancini M *et al* 2015 *Science* **349** 1510
[63] Chiu C S, Ji G, Mazurenko A, Greif D and Greiner M 2018 *Phys. Rev. Lett* **120** 243201
[64] Bonnes L, Hazzard K R A, Manmana S R, Rey A M and Wessel S 2012 *Phys. Rev. Lett.* **109** 205305
[65] Hazzard K R A, Gurarie V, Hermele M and Rey A M 2012 *Phys. Rev.* A **85** 041604
[66] Ozawa H, Taie S, Takasu Y and Takahashi Y 2018 *Phys. Rev. Lett.* **121** 225303
[67] Hofrichter C, Riegger L, Scazza F, Höfer M, Fernandes D R, Bloch I and Fölling S 2016 *Phys. Rev.* X **6** 021030
[68] Taie S, Yamazaki R, Sugawa S and Takahashi Y 2012 *Nat. Phys.* **8** 825
[69] Hikami S, Larkin A I and Nagaoka Y 1980 *Prog. Theor. Phys.* **63** 707
[70] Brouwer P W, Duckheim M, Romito A and von Oppen F 2011 *Phys. Rev. Lett.* **107** 196804
[71] Bir G and Pikus G 1974 *Symmetry and Strain-Induced Effects in Semiconductors* (New York : Wiley)
[72] Kittel C 1963 *Quantum Theory of Solids* (New York : Wiley)
[73] Bardeen J, Cooper L N and Schrieffer J R 1957 *Phys. Rev.* **108** 1175
[74] Blaizot J and Ripka G 1986 *Quantum Theory of Finite Systems* (Cambridge, MA: MIT Press)
[75] Zubarev D N 1960 *Phys.—Usp.* **3** 320